Metacarpophalangeal Joints of the Long Fingers : Anatomy, Biomechanics, and Imaging Techniques

Bouredoucen, Hicham; Boudabbous, Sana; Poletti, Pierre-Alexandre Alois; Taihi, Lokmane

How to cite

BOUREDOUCEN, Hicham et al. Metacarpophalangeal Joints of the Long Fingers : Anatomy, Biomechanics, and Imaging Techniques. In: European journal of radiology, 2026, vol. 194, p. 112459. doi: 10.1016/j.ejrad.2025.112459

This publication URL: https://archive-ouverte.unige.ch/unige:192529
Publication DOI: 10.1016/j.ejrad.2025.112459

European Journal of Radiology 194 (2026) 112459

Contents lists available at ScienceDirect

European Journal of Radiology

journal homepage: www.elsevier.com/locate/ejrad

Review

Metacarpophalangeal Joints of the Long Fingers: Anatomy, Biomechanics, and Imaging Techniques

Hicham Bouredoucen [a,1,*], Sana Boudabbous [a,2], Pierre-Alexandre Poletti [a,3], Lokmane Taihi [b,4]

[a] Division of Radiology, Department of Imaging and Medical Informatics, Geneva University Hospitals, University of Geneva, Geneva, Switzerland
[b] Medical Imaging, Cliniques Universitaires Saint Luc, Brussels,Belgium

ARTICLE INFO

Keywords:
Metacarpophalangeal joint
Finger
Anatomy
Biomechanics
Sagittal band
Collateral ligament
MRI
Ultrasound

ABSTRACT

Introduction: The metacarpophalangeal joint (MCPJ) of the long fingers is essential for various hand functions. Joint kinematics are complex, involving flexion-extension, lateral movements, and axial rotation. During these motions, different joint stresses occur. The long finger MCPJ operates through a balance between mobility on one hand and stability and joint congruence on the other. Anatomical structures ensuring this balance through adaptive biomechanical mechanisms include the articular surfaces, which provide minimal stabilization except at the terminal degrees of flexion; the capsulo-ligamentous system, which acts as the primary stabilizer by maintaining constant joint tension; and the musculo-tendinous system, which ensures stability during movement. An anatomo-biomechanical and imaging approach facilitates the understanding of the physiological and pathological aspects of the long finger MCPJ and contributes to improved therapeutic strategies. The aim of this article is to provide a detailed description of the normal anatomy and biomechanics of the MCPJ of the long fingers, correlated with imaging, in order to improve the understanding of physiological and pathological aspects.

Methodology: This educational review presents the normal anatomy and biomechanics of the long finger MCPJ through imaging. The various components of the MCPJ of the long fingers are detailed, including articular surfaces, capsule, collateral ligaments, deep transverse metacarpal ligament, volar plate, dorsal triangular fibrocartilage, dorsal hood, extensor tendons, sagittal bands, and the interosseous and lumbrical muscles. In addition to standard radiography, several imaging modalities are used to evaluate the MCPJ of the long fingers. Dynamic conventional radiography assesses joint stability. Computed tomography (CT) or cone-beam CT (CBCT) can complement the assessment. High-resolution ultrasound (US) is well suited for dynamic studies. High-field 3T magnetic resonance imaging (MRI) provides excellent spatial resolution and contrast.

Results and conclusion:: A thorough knowledge of anatomy and biomechanics is essential for the imaging analysis of the MCPJ of the long fingers and forms the basis for exploring both normal and pathological aspects.

Abbreviations: A1, A1 pulley; aCL, Accessory collateral ligament; aRCL, Accessory radial collateral ligament; aUCL, Accessory ulnar collateral ligament; DTML, Deep transverse metacarpal ligament; CL, Collateral ligaments; CBCT, Cone-Beam CT; ET, Extensor tendon; FT, Flexor tendons; MRI, Magnetic resonance imaging; MC, Metacarpal; MCPJ, Metacarpophalangeal joint; pCL, Principal collateral ligament; pRCL, Principal radial collatéral ligament; pUCL, Principal ullnar collatéral ligament; P1, Proximal phalanx; RCL, Radial collateral ligament; SB, Sagittal bands; UCL, Ulnar collateral ligament; US, Ultrasound; VP, Volar plate.

* Corresponding author at: : Division of Radiology, Department of Imaging and Medical Informatics, Geneva University Hospitals, Rue Gabrielle-Perret-Gentil 4 1211 Geneva 14, Switzerland.

E-mail addresses: bour_hich@hotmail.com (H. Bouredoucen), Sana.Boudabbous@hug.ch (S. Boudabbous), Pierre-Alexandre.Poletti@hug.ch (P.-A. Poletti), lokmane.taihi@saintluc.uclouvain.be (L. Taihi).

[1] orcid.org/0009-0003-1826-6827
[2] orcid.org/0000-0003-0516-4613
[3] orcid.org/0000-0001-9214-5546
[4] orcid.org/0000-0001-9286-3783

https://doi.org/10.1016/j.ejrad.2025.112459
Received 9 July 2025; Received in revised form 6 September 2025; Accepted 26 September 2025
Available online 30 September 2025

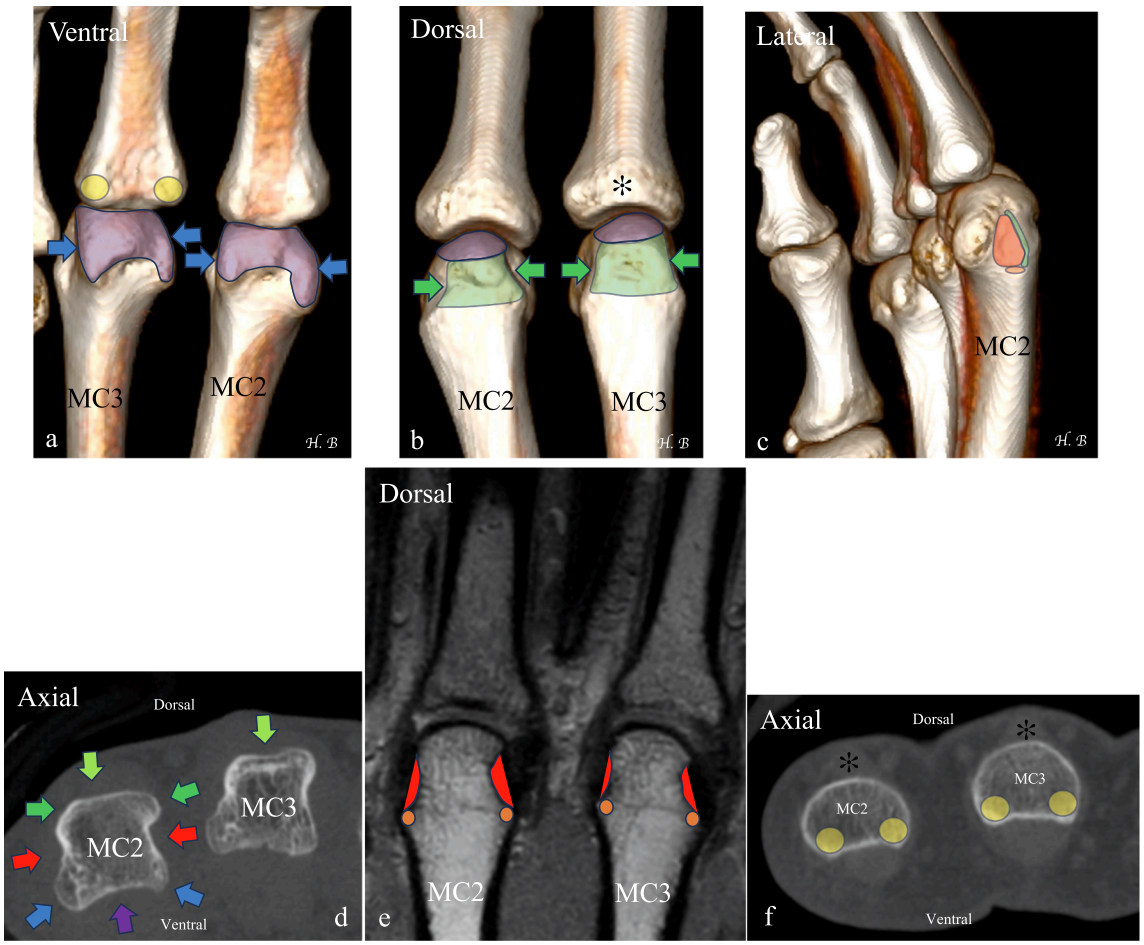

Fig. 1. Bony anatomy of the MCPJ of the long fingers (a–f). CBCT volume-rendered reconstructions (a, b, c), axial CBCT images (d, f), coronal T1-weighted MRI (e). Bony anatomy of the metacarpal head (a–e): The volar aspect of the metacarpal head is spherical and covered with cartilage (a, purple - palmar side). The dorsal aspect shows cartilage only on its upper portion (b, purple - dorsal side). The posterior surface is articular but noncartilaginous (b, green), flat or slightly concave where the extensor tendon passes. The volar side is bordered by two prominent, mildly convex and blunt bony ridges (a, blue arrows), while the dorsal border presents two sharper, more prominent lateral crests that are slightly concave outward (b, green arrows) and end in an inferior pointed tip (b). On the medial and lateral sides, a small fossa (c, red) is located anterior to the posterior crest (c, green) and ends inferiorly in a tubercle (c, orange); the collateral ligament inserts onto both the fossa and the tubercle. The metacarpal head is asymmetrical, with the articular surface being more extensive on the radial side than on the ulnar side. On the axial CBCT view (d), the anterior borders (blue arrows) are blunt, while the posterior borders (dark green arrows) are sharp. The anterior articular surface (purple arrow) is convex; the posterior surface (light green arrows) is flat or slightly concave. The two lateral fossae are visible (red arrows). Metacarpal head anatomy on MRI (e): MRI section through the center of the metacarpal head shows the lateral fossa (red) and tubercle (orange), with the collateral ligament inserting at both points. Bony anatomy of the base of the proximal phalanx (P1) (a, b, c, f): The base of P1 has a parallelepiped shape with a concave articular surface forming the glenoid cavity. The volar surface is concave to accommodate the flexor tendons (a). On this volar surface, there are two bony protrusions where the volar plate inserts (yellow, a). The dorsal surface is smooth and convex (asterisk, b). In (f), the same features are seen: a smooth, convex dorsal surface (asterisk), a volar surface with two bony prominences (yellow) where the volar plate inserts, and a concavity for the flexor tendons.

1. Introduction

The metacarpophalangeal joint (MCPJ) of the long fingers exhibits complex joint kinematics, including flexion-extension, lateral movements, and axial rotation. It functions through a balance between mobility on one hand and stability and joint congruence on the other. The anatomical structures that ensure this balance through adaptive biomechanical mechanisms are the articular surfaces, the capsuloligamentous system, and the musculotendinous system [1].

There are several challenges in understanding the complex anatomy of the long finger MCPJ, which have important diagnostic and therapeutic implications. The metacarpal (MC) head has specific anatomical features relevant to the analysis of standard radiographs: the two bony prominences on the palmar aspect are slightly convex, while the two lateral ridges on the dorsal aspect are slightly concave. The articular surface is more extensive on the radial longitudinal side than on the ulnar side. The distribution of the cartilaginous surface of the MC head is variable; its ventral side presents a broader cartilaginous articular surface, whereas its dorsal side includes only a superior cartilaginous portion [2]. The normal anatomical insertions of the proximal dorsal MC and distal palmar phalangeal attachments of the ulnar collateral ligament (UCL) and radial collateral ligament (RCL), along with their oblique course [3–5], can lead to misdiagnosis of tears on ultrasound (US) or magnetic resonance imaging (MRI) if not assessed in their true anatomical planes. The collateral ligaments (CL) of the index finger MCPJ exhibit the greatest obliquity in the sagittal plane, which decreases in the ulnar fingers, where the principal collateral ligament (pCL) is more closely aligned with the long axis of the proximal phalanx (P1) [5], emphasizing the need to study them in the correct imaging planes. Each pCL and accessory collateral ligament (aCL) is actually composed of three anatomo-functional parts (dorsal, middle, and palmar), whose functions and roles in joint stability differ and are important to recognize [4,6]. The “Zancolli assembly nucleus” is a continuum formed by the aggregation of multiple fibers originating from

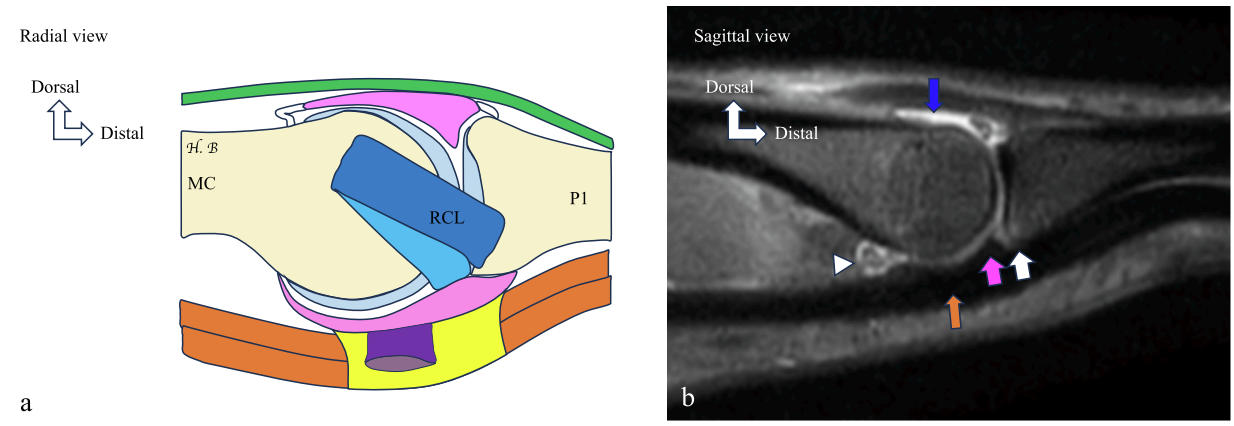

Fig. 2. Articular recesses of the index finger MCPJ. Schematic drawing (a). Sagittal PD FS MRI (b) showing joint effusion in the dorsal recess (blue arrow) of the MCPJ articular cavity in the setting of a ligamentous sprain with reactive joint effusion. Volar plate (pink arrow). The distal volar recess of the MCPJ articular cavity (white arrow) shows no significant effusion; the distal recess and flexor tendons (orange arrow) are compressed. The proximal volar recess of the MCPJ articular cavity (arrowhead) is lax and contains a small joint effusion. MC, metacarpal; P1, proximal phalanx; RCL, radial collateral ligament.

the volar plate (VP), sagittal bands (SB), CL, the A1, and the deep transverse metacarpal ligament (DTML), making their convergence difficult to distinguish on imaging [7,8].

This article aims to provide a comprehensive overview of the normal anatomy and biomechanics of the long finger MCPJ, in correlation with imaging, to improve the understanding of both physiological and pathological conditions.

2. Anatomy and biomechanics of the MCPJ of the long fingers

The MCPJ of the long fingers exhibits complex joint kinematics with three degrees of freedom. Flexion-extension is the primary degree of freedom, ranging from 15° in extension to 90° in flexion. The main muscles responsible for flexion are the palmar and dorsal interossei. The extrinsic flexors do not act directly on the MCPJ. Extension is performed by the extensor digitorum communis through its central capsular fibers. In lateral movements, ulnar deviation (20° to 40°) is significantly greater than radial deviation (10° to 20°). This lateral inclination occurs only in extension and completely disappears in flexion. The DTML limits medial and lateral mobility. Axial rotation (frontal plane tilt) exhibits variable amplitude. The MCPJ of the long fingers must balance mobility on one side and stability and joint congruence on the other. Three components contribute to this balance. The articular shapes themselves provide minimal stabilization except at the end range of flexion. The capsuloligamentous system acts as the primary stabilizer and ensures permanent stability. CL provide 70% of rotational stability; 60% of anteroposterior stability (palmar glide of P1); and 90% of lateral stability [9]. The VP ensures anteroposterior congruence by preventing posterior subluxation of P1. The musculotendinous system ensures stability during movement.

2.1. Anatomy and biomechanics of the bony structures and articular surfaces of the MCPJ of the long fingers

The MCPJ of the long fingers is a condyloid (enarthrosis-type) joint formed by the articular surfaces of the MC head and the glenoid cavity of the base of the P1.

2.1.1. The metacarpal head (Fig. 1, a, b, c, d, e).

The MC head has a complex shape. Its articular surface is convex, extending more in the anteroposterior direction than transversely, and is larger on the palmar side than on the dorsal side. The palmar surface is spherical and covered with cartilage. The dorsal surface is rough, with only the superior portion being cartilaginous. The posterior surface is articular but non-cartilaginous and is either flat or slightly concave where the extensor tendon (ET) passes. The palmar side is bordered by two bony ridges along the ulnar and radial edges, which are slightly convex and blunt. In contrast, the dorsal border features two sharper lateral crests, slightly concave outward in relation to the MC axis, ending in an inferior point. The lateral and medial sides of the MC head are relatively flattened, each containing a fossa located anterior to the posterior crest. The proximal dorsal apex of this fossa ends in a tubercle where the collateral ligament inserts. The MC head is asymmetrical, with the articular surface extending more on the radial longitudinal side than on the ulnar side. This bony and articular anatomy is well demonstrated on axial Cone-Beam CT (CBCT) and coronal MRI images.

2.1.2. The base of the proximal phalanx (Fig. 1, a, b, c, f).

The base of P1 has a parallelepiped shape with a concave articular surface forming a glenoid cavity oriented primarily along the transverse axis. It covers only about one-third of the MC articular surface. The dorsal surface of P1 is smooth and convex. The ventral surface is concave at the passage of the flexor tendons (FT). On this ventral face, a bony ridge with two prominences serves as the insertion site for the VP. This anatomy is illustrated on axial CBCT images.

2.1.3. Articular capsule (Fig. 2)

The capsule surrounding the MCPJ is thin and highly lax, with articular recesses more prominently developed dorsally [10].

2.2. Anatomy and biomechanics of the ligamentous structures, volar plate, and dorsal triangular fibrocartilage of the MCPJ of the long fingers

2.2.1. Collateral ligaments of the MCPJ (Fig. 3)

The RCL is thicker and stiffer than the UCL. Each ligament consists of two distinct bundles: the pCL and the aCL. They originate from fossae on the radial and ulnar sides of the MC head and extend distally toward the base of the P1. The principal radial collateral ligament (pRCL) arises from the dorso-radial surface of the MC head and inserts onto the lateral tubercle of P1. The principal ulnar collateral ligament (pUCL) arises from the dorso-ulnar surface of the MC head and inserts onto the palmar-proximal surface of P1. The accessory ulnar collateral ligament (aUCL) and accessory radial collateral ligament (aRCL) share the same MC origin as their corresponding proper CL; they extend palmarly and are firmly attached distally to the VP. In the index and middle fingers, the MC head is circular in the sagittal plane and trapezoidal in the coronal plane [11]. Due to this cam-like shape of the MC head, when the MCPJ flexes further, the collateral ligament tightens because the distance between the two ligament ends increases as it passes over the condyles of the MC head. This mechanism contributes to enhanced joint stability

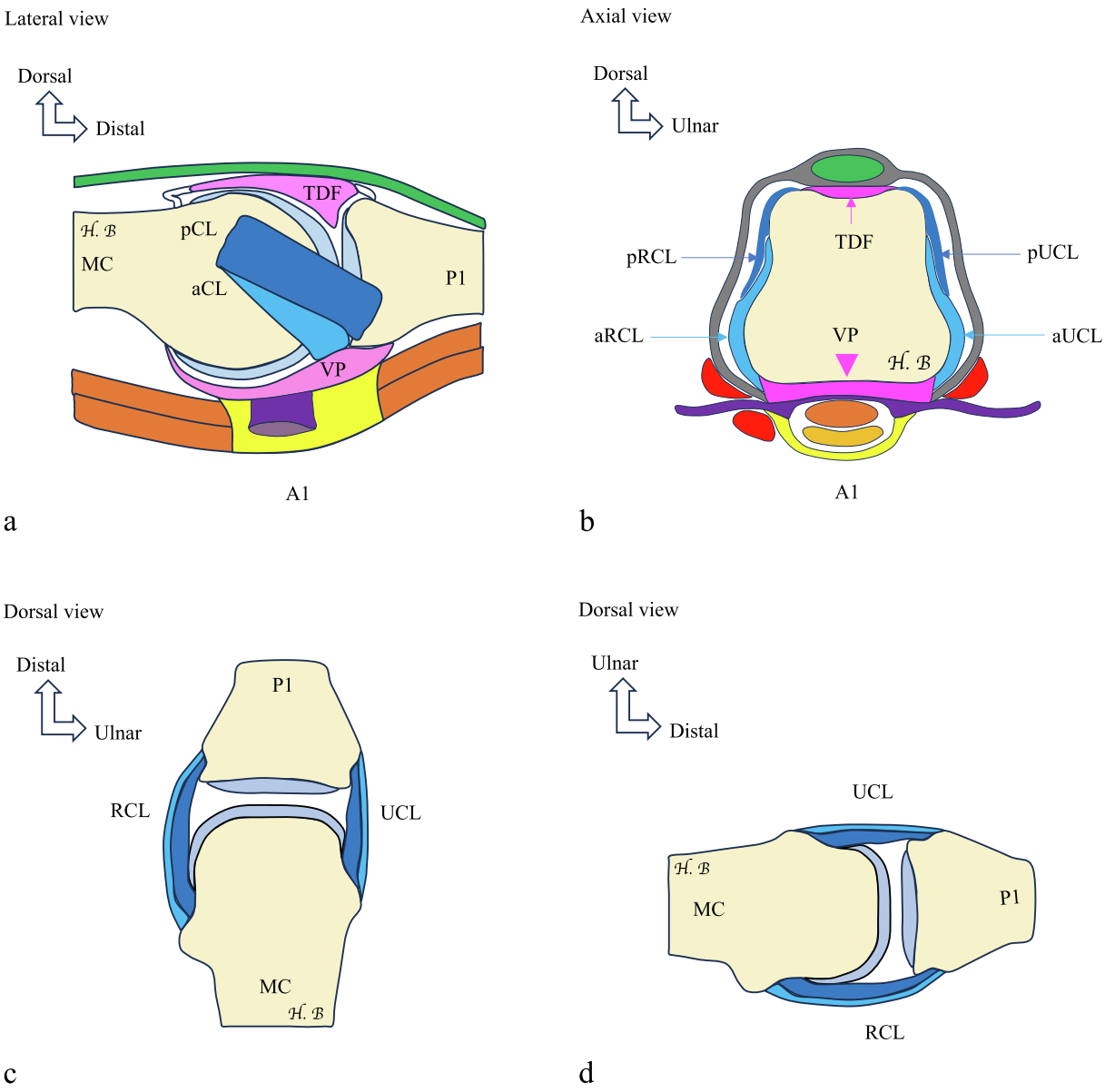

Fig. 3. Collateral ligaments of the index finger MCPJ. Illustration showing the anatomical structures of the collateral ligaments of the MCPJ of the index finger. The pCL originates from the metacarpal and inserts on the base of the P1, while the aCL extends toward the volar plate. MC, metacarpal; P1, proximal phalanx; pCL, proper collateral ligament; aCL, accessory collateral ligament; aRCL, accessory radial collateral ligament; UCL, accessory ulnar collateral ligament; pRCL, principal radial collatéral ligament; pUCL, principal ullnar collatéral ligament; TDF, triangular dorsal fibrocartilage; A1, A1 pulley; VP, volar plate; RCL, radial collateral ligament; UCL, ulnar collateral ligament.

(Fig. 4). In the ring and little fingers, the distance between the ligament ends remains constant, so there is no increase in CL tension during MCPJ flexion [12]. As the MCPJ flexion angle increases, tension in both the RCL and UCL increases; therefore, collateral ligament instability testing should be performed with the MCPJ in flexion [13,14]. The pCL is taut during flexion (Fig. 4a, b) and relaxed during extension (Fig. 4c, f). The pCL is composed of three anatomo-functional parts that play distinct roles in joint stability [4]. The dorsal and middle portions of the CL are tensioned during flexion and relaxed during extension [4,5]. The middle portion of the CL remains nearly isometric between 60° and 90° of flexion. Conversely, the palmar portion of the CL is more tensioned in extension than in full flexion, and is relaxed from 30° to 90° of flexion. This relaxation permits a greater lateral range of motion, allowing abduction and adduction [4]. The aCL [6] is taut in extension (Fig. 4c, d) and relaxed in flexion (Fig. 4a, b). It is also composed of three anatomofunctional parts: the dorsal and middle portions are isometric, while the palmar portion is tensioned in extension.

2.2.2. *Deep transverse metacarpal ligament (Fig. 5)*

The DTML extends from the second to the fifth metacarpals in a radio-ulnar direction, crossing the palmar aspect of the MCPJ. It is absent on the radial side of the index finger and the ulnar side of the little finger. It is a strong fibrous band that stabilizes the MC heads and maintains the transverse MC arch. Its integrity is essential for grip strength [15]. It allows palmar and dorsal mobility as well as limited rotation, while restricting medial and lateral displacement [16]. The FT, neurovascular bundles, and lumbricals muscles are located on the volar surface of the DTML, while the interossei muscles lie on its dorsal or deep surface. Its posterior surface is connected to the VP and serves as a link between them, while its grooved volar surface interfaces with the flexor tendons. The SB insert into the dorsal portion of the DTML. The A1 inserts into the volar grooves of the DTML [15]. The so-called “Zancolli

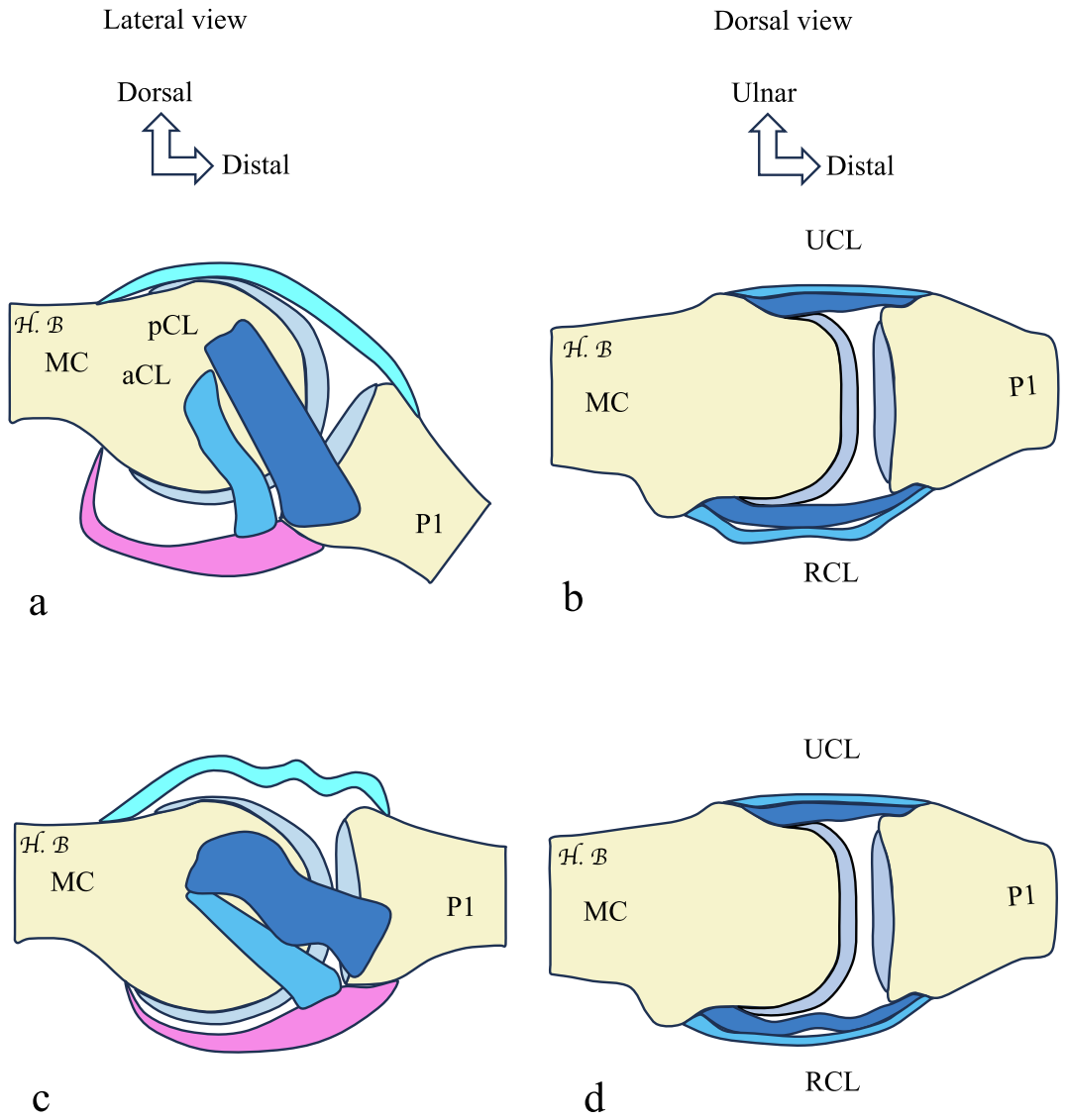

Fig. 4. Biomechanics of the collateral ligament of the index finger MCPJ. In the index and middle fingers, the trapezoidal cam-shaped contour of the metacarpal head in the coronal plane contributes to tensioning the collateral ligament bundles and enhancing joint stability. During MCPJ flexion (a, b), the pCL is taut, while the aCL is relaxed. During MCPJ extension (c, d), the aCL becomes taut, and the pCL is relaxed. Note that the pCL inserts on the base of the P1, while the aCL attaches to the volar plate (shown in pink). MC, metacarpal; P1, proximal phalanx; pCL, proper collateral ligament; aCL, accessory collateral ligament; RCL, radial collateral ligament; UCL, ulnar collateral ligament.

assembly core" refers to a structural continuum resulting from the convergence of fibers from the VP, SB, CL, A1, and the DTML [7].

2.2.3. The Volar plate of the MCPJ (Fig. 6)

The VP consists of a main body, two thin and elastic proximal attachments (check rein ligaments) that insert on the lateral edges of the MC body, a distal portion composed of two thick and rigid distal attachments that insert on the volar surface of the base of the P1, and a thin central zone that contains a synovial recess on its deep surface [17]. A central distal notch is present between the two solid attachments. The posterior surface of the VP is articular and concave, while its anterior, non-articular surface is grooved to provide a gliding surface for the FT. The A1 attaches to the lateral edges of the metacarpophalangeal VP and extends to the base of the P1. Small sesamoid bones may be inconsistently present within the VP, particularly in the second and fifth rays.

2.2.4. Triangular dorsal fibrocartilage of the MCPJ (Fig. 3)

It is a dorsal structure, crescent-shaped in the coronal plane and triangular in the sagittal plane. It is attached to the ET by strands of Landsmeer's intertendinous fascia. Dorsally, it is continuous with and attached to the joint capsule. On its volar surface, it consists of two synovial recesses, a proximal one extending to the MC diaphysis and a distal one extending to the P1. The functions of the triangular dorsal fibrocartilage of the MCPJ are to stabilize the ET and the MCPJ itself [18].

2.3. Anatomy and biomechanics of muscular and tendinous structures

2.3.1. Sagittal bands

The extensor hood stabilizes the ET on the dorsal aspect of the MCPJ, as well as on the P1 and middle phalanges. It is composed of three retinacular bands arranged from proximal to distal: sagittal, transverse, and oblique bands (Fig. 7). The SB divides dorsally to envelop the ET in a tunnel formed by thin superficial layers and thicker deep layers [19,20]. Laterally to the ET, these layers fuse to form radial and ulnar laminae [19]. In the mid-lateral zone, SB fibers lie superficially to the pCL [21]. The SB joins the VP to form a closed cylindrical tube encasing the MC head and the MCPJ. It merges palmarly with the VP, the insertion of the

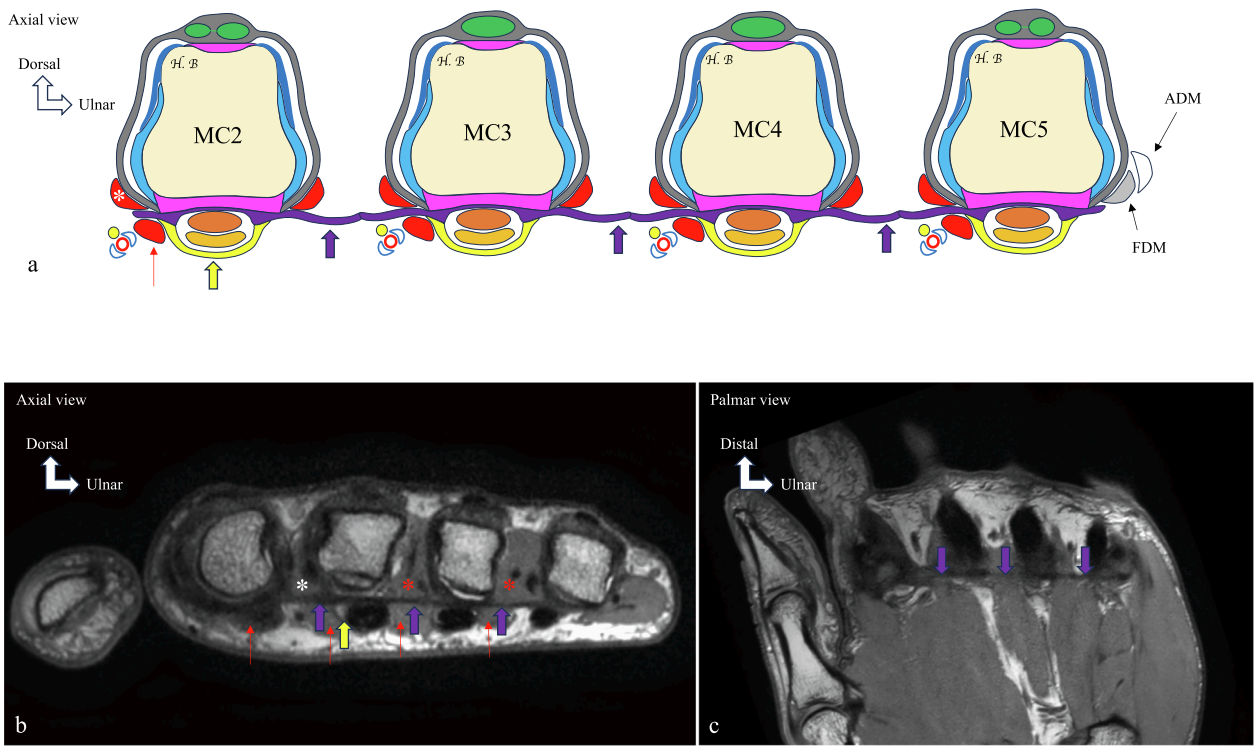

Fig. 5. Deep transverse metacarpal ligament. Schematic transverse drawing of the long fingers MCPJ (a), axial (b) and coronal (c) PD MRI images. Deep transverse metacarpal ligament (purple arrow), A1 pulley (yellow arrow), lumbrical muscles (red arrows), interosseous muscles (asterisk). ADM, Abductor digiti minimi; FDM, Flexor digiti minimi.

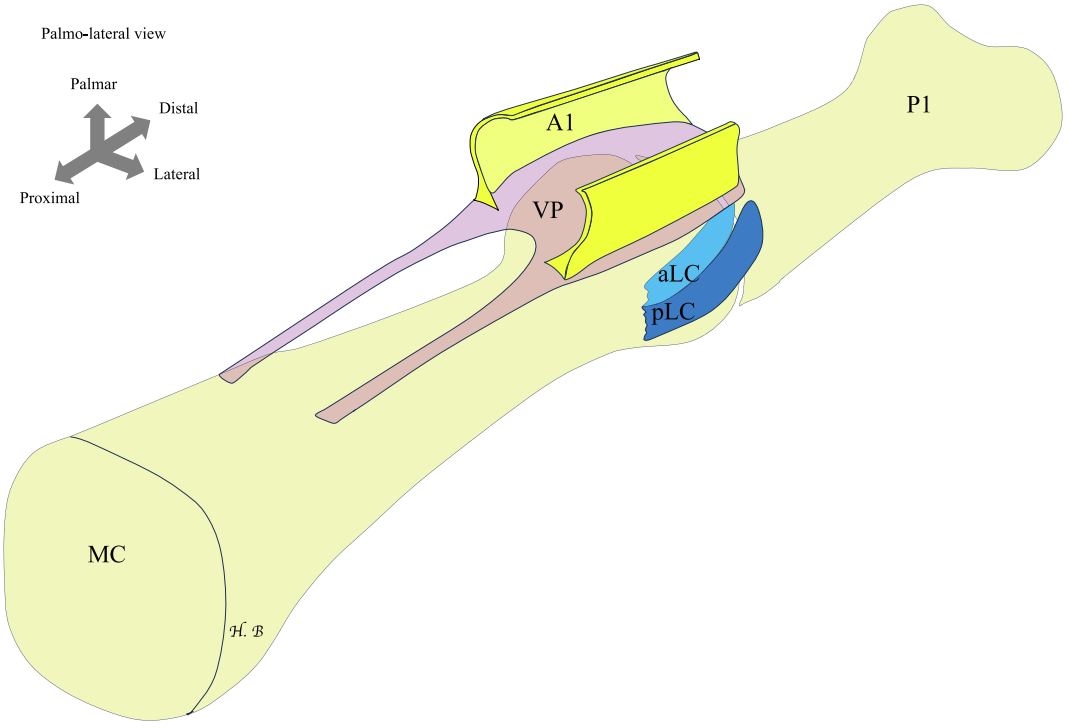

Fig. 6. Volar plate of the long fingers MCPJ. Schematic drawing. The volar plate (VP) consists of a body providing a gliding surface for the flexor tendons, two thin and elastic proximal attachments (check reins) inserting on the lateral edges of the metacarpal (MC) body, and a distal portion composed of two thick, rigid distal attachments inserting on the palmar aspect of the base of the proximal phalanx (P1). A thin central zone houses a synovial recess on its deep surface. The posterior surface of the VP is articular and concave; the anterior, non-articular surface features a groove through which the flexor tendons glide. The VP is connected to the accessory collateral ligaments (aCL). The A1 pulley corresponds to the beginning of the digital tunnel; it originates and attaches to the lateral edges of the VP at the MCPJ and extends to the base of P1. Principal collateral ligaments (pCL).

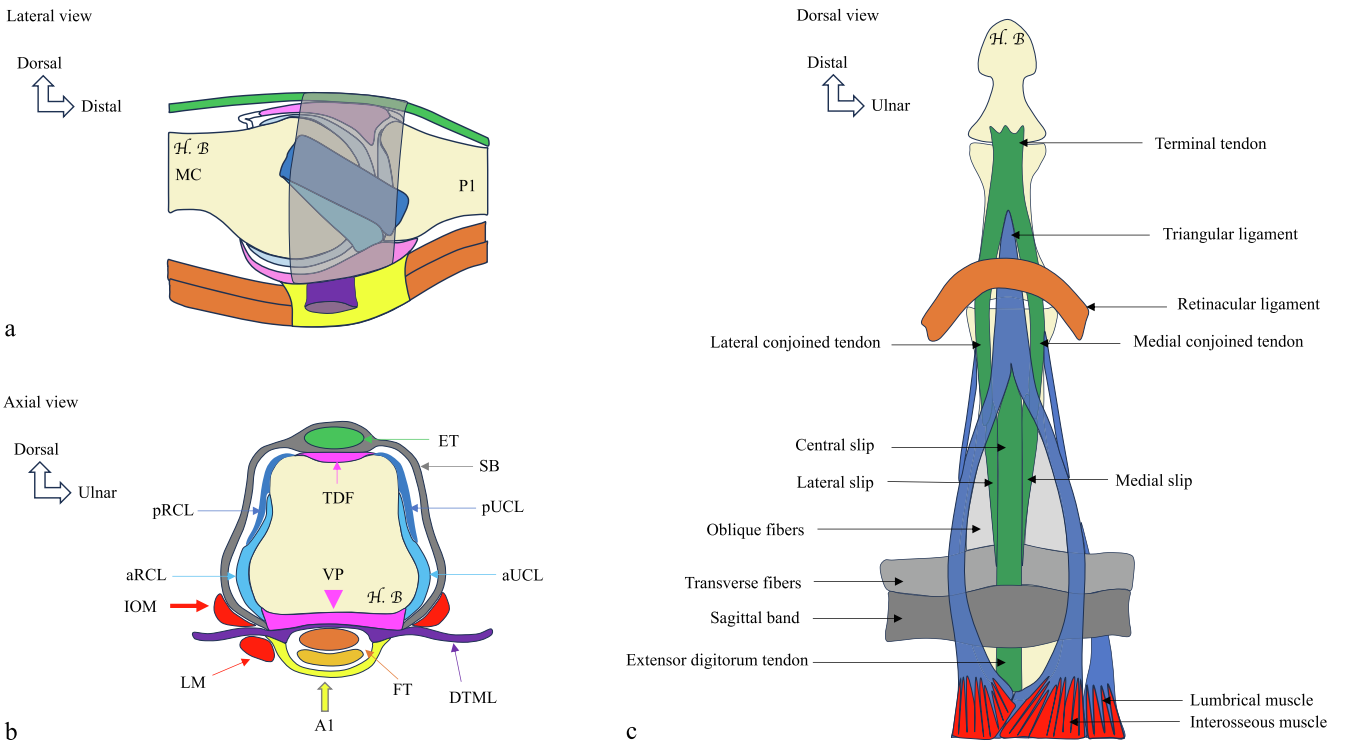

Fig. 7. Collateral ligaments of the MCPJ of the long fingers, dorsal hood, sagittal bands, and extensor apparatus. Schematic drawings. Collateral ligaments, sagittal bands, and extensor apparatus in lateral view (a) and axial view (b). The extensor apparatus and dorsal hood in dorsal view (c). The dorsal hood is composed of three main stabilizing retinacular bands arranged from proximal to distal: sagittal, transverse, and oblique bands. MC, metacarpal; P1, proximal phalanx; ET, extensor tendon; TDF, triangular dorsal fibrocartilage; pRCL, principal radial collatéral ligament; pUCL, principal ullnar collatéral ligament; aRCL, accessory radial collateral ligament; aUCL, accessory ulnar collateral ligament; SB, sagittal bands; FT, flexor tendons; VP, volar plate; A1, A1 pulley; DTML, deep transverse metacarpal ligament; IOM, interosseous muscles; LM, lumbrical Muscles.

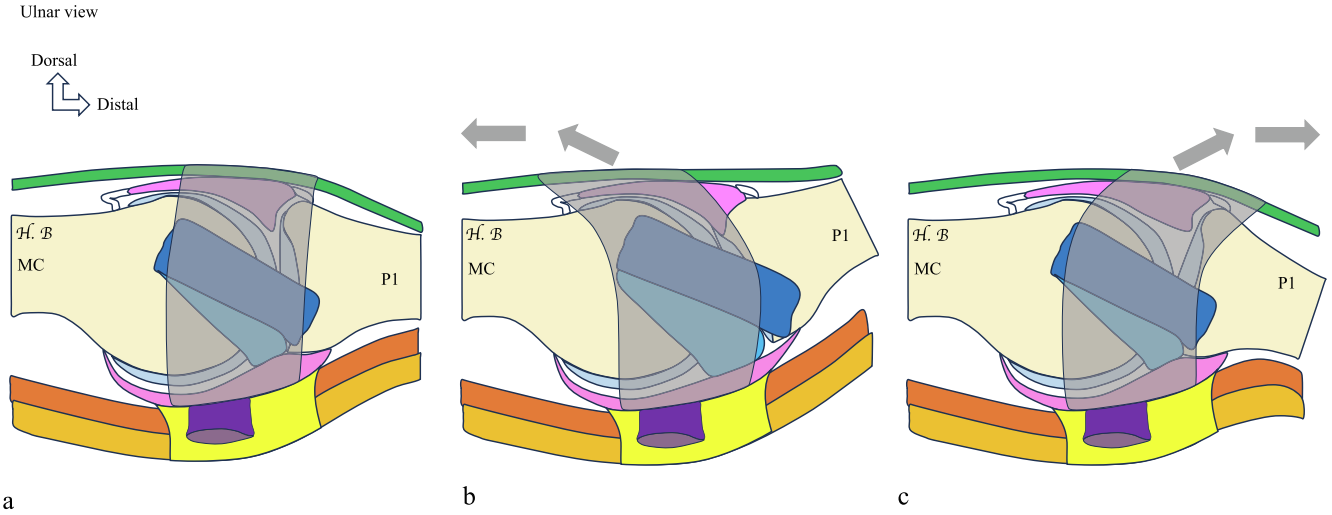

Fig. 8. Biomechanics of the sagittal band during MCPJ extension and flexion in the long fingers. Schematic illustrations showing: In the neutral position, the SB is relaxed *(a)*. In the extension mechanism of the MCPJ *(b)*, during hyperextension, the SB shifts from distal to proximal and becomes taut, limiting proximal excursion of the extensor tendon. In the flexed position *(c)*, the SB moves from proximal to distal along with MCPJ motion. The radial SB is subjected to greater tensile stress during ulnar deviation and MCPJ flexion. MC, metacarpal; P1, proximal phalanx; SB, sagittal band.

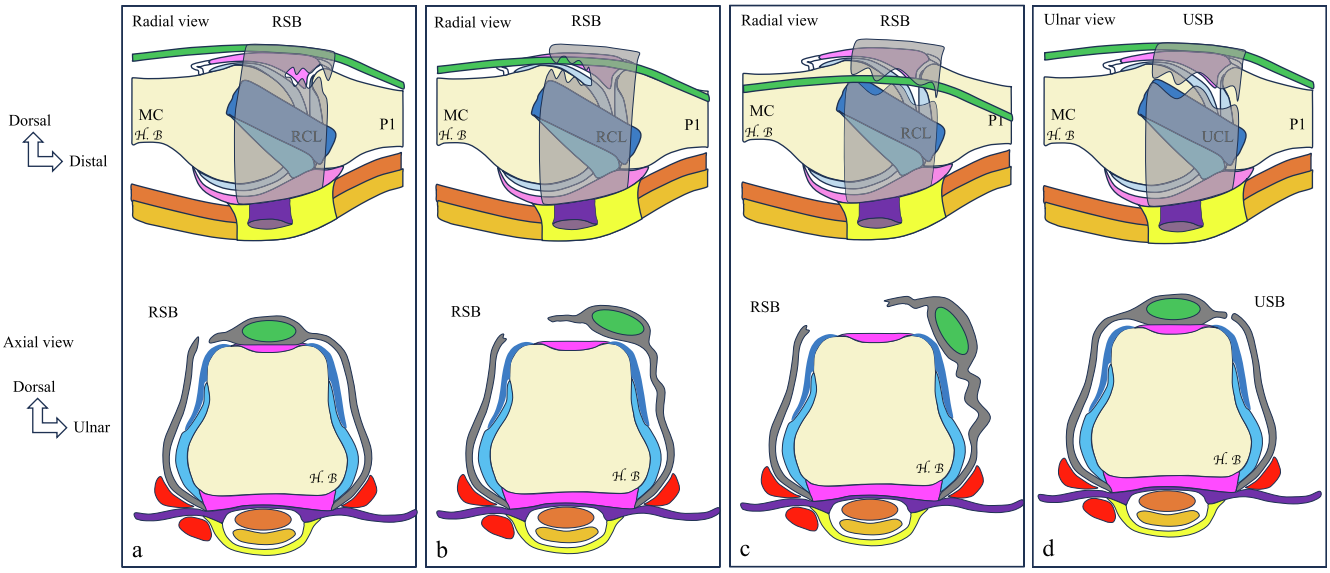

Fig. 9. Effects of sagittal band injuries on extensor tendon stability at the MCPJ of the long fingers. Schematic illustrations: Rupture of the distal half of the RSB does not result in ET instability *(a)*. Rupture of the proximal half of the RSB leads to subluxation of the ET *(b)*. Complete rupture of the RSB causes dislocation of the ET *(c)*. Rupture of the USB does not cause ET instability *(d)*.Tendon instability has been shown to increase with the MCPJ flexion, particularly between 45° and 90°, and with wrist flexion beyond the neutral position. MC, metacarpal; P1, proximal phalanx; RSB, radial sagittal band; USB, ulnar sagittal band; SB, sagittal band; ET, extensor tendon.

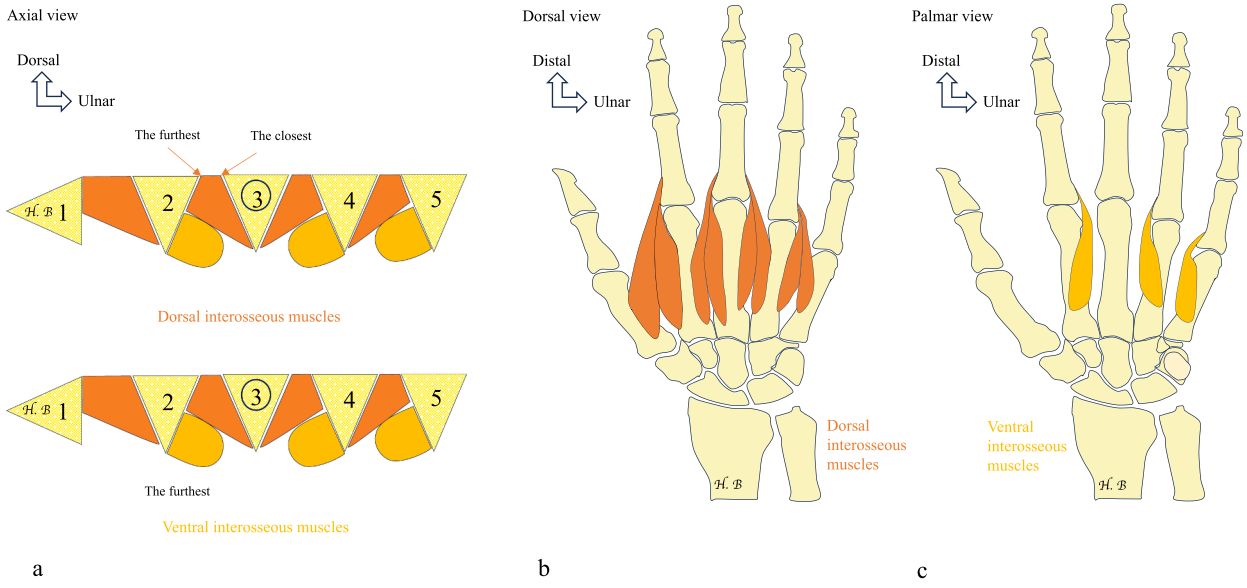

Fig. 10. Anatomy of the proximal insertions of the interosseous muscles. Schematic illustration. There are four dorsal interosseous muscles. Their proximal insertions (a, b) consist of two groups of fibers: the first group inserts on the lateral surface of the metacarpal closest to the middle finger, and the second group on the lateral surface of the metacarpal farthest from the middle finger. There are three palmar interosseous muscles. Their proximal insertions (a, c) are located on the lateral surface of the metacarpal farthest from the middle finger.

aCL, the flexor tendon sheath, A1, and the DTML [19]. The SB is the primary stabilizer of the ET on the dorsal aspect of the MCPJ during flexion and extension. It limits tendon excursion, subluxation, or dislocation, prevents bowstringing of the ET, and participates in P1 extension [21–23]. The SB is a dynamic structure: its fibers move with the ET during MCPJ motion (Fig. 8) [21]. Radial SB rupture typically occurs under stress—most often during forced ulnar deviation, resisted extension, or, less frequently, during flexion [21]. When the SB is torn, the tendon subluxes or dislocates to the side opposite the injury due to the unopposed tension from the intact contralateral band. The radial SB is more commonly injured, as it is thinner and longer than the ulnar SB [19,24]. Rupture of the distal half of the radial lamina does not cause ET instability. Rupture of the proximal half involving at least 50% leads to subluxation. Complete rupture of the radial lamina results in dislocation (Fig. 9) [21]. Complete rupture of the radial SB causes ET instability in the index, middle, and ring fingers. This injury most frequently affects the middle finger, due to the prominence of the MC head (Fig. 8, 9) [20,25,26]. In contrast, partial or complete rupture of the ulnar lamina does not cause instability (Fig. 9) [21].

2.3.2. *Interosseous muscles*

There are four dorsal interosseous muscles, with proximal dorsal

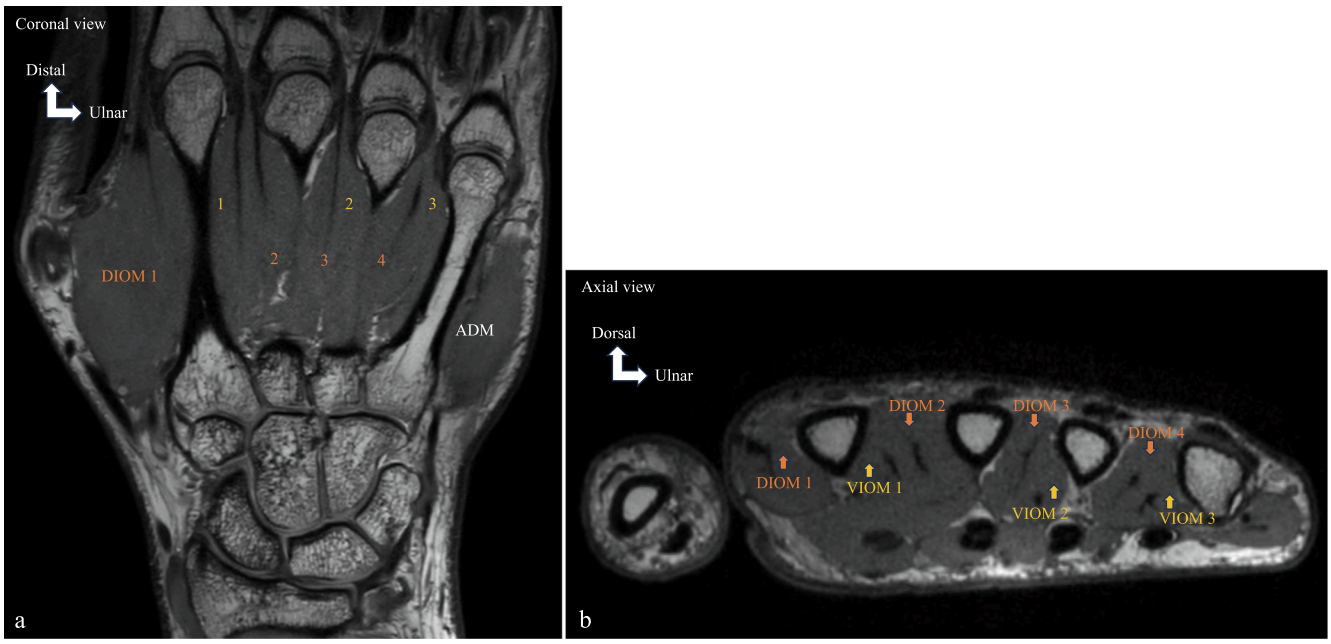

Fig. 11. MRI showing the proximal insertions of the dorsal and palmar interosseous muscles. Coronal (a) and axial (b) proton density (PD) MRI sequences. Dorsal interosseous muscles are shown in dark red; palmar interosseous muscles in light orange. VIOM 1, First ventral interosseous muscle; VIOM 2, Second ventral interosseous muscle; VIOM 3, Third ventral interosseous muscle; DIOM 1, First dorsal interosseous muscle; DIOM 2, Second dorsal interosseous muscle; DIOM 3, Third dorsal interosseous muscle; DIOM 4, Fourth dorsal interosseous muscle; ADM, Abductor digiti minimi.

insertions (Figs. 10, 11) consisting of two groups of fibers : the first group inserts on the lateral surface of the MC closest to the middle finger, the second group inserts on the lateral surface of the MC farthest from the middle finger. There are three ventral interosseous muscles, with proximal palmar insertions (Figs. 10, 11) on the lateral surface of the MC farthest from the middle finger. The interosseous muscles also have distal insertions (Figs. 12, 13), both deep and superficial. The deep insertions are capsular, attaching to the distal part of the VP of the MCPJ, and sometimes to the tubercle at the base of the P1. The superficial insertion connects to the extensor apparatus and is divided into three parts : the proximal part (interosseous hood) merges with the lateral edge of the ET and the joint capsule of the MCPJ; proximally, this hood also covers the SB; the middle part (fan fibers) inserts onto the ET at the level of P1; the distal part divides into three fibers. Functionally, through their deep insertions, the interossei control finger lateral movements : the dorsal interossei abduct, while the ventral interossei adduct the fingers. Through their superficial insertions, they contribute to MCPJ flexion and extension of both the proximal and distal interphalangeal joints.

2.3.3. Lumbrical muscles

There are four lumbrical muscles. Their proximal insertions (Figs. 14, 15) are as follows: the first lumbrical originates from the radial border of the flexor digitorum profundus tendon of the index finger; the second lumbrical arises from the radial border of the flexor digitorum profundus tendon of the middle finger; the third and fourth lumbricals are bipennate: the third originates from the flexor digitorum profundus tendons of the middle and ring fingers; the fourth originates from the flexor digitorum profundus tendons of the ring and little fingers. The lumbrical tendon courses through the interdigital space, passes palmar to the DTML, then turns dorsally around the finger to merge with the superficial fascicle of the interosseous tendon (intrinsic lateral band) (Fig. 16). It ultimately inserts on the radial lateral band of the ET, which continues to the base of the distal phalanx (distal insertion) (Fig. 16). Like the interosseous muscles, the lumbricals contribute to extension of the proximal and distal interphalangeal joints. They play an essential role in coordinating the flexor and extensor systems of the fingers [27–30].

3. The value of anatomical knowledge in clinical practice

It is essential to understand the anatomy of the MC head. Its palmar surface is defined by two osseous prominences along the ulnar and radial borders, which are slightly convex and blunt, whereas the dorsal surface is characterized by two sharper, slightly concave lateral ridges [2]. In the assessment of erosive arthropathy, such as rheumatoid arthritis, erosions should be sought on both the prominences and the ridges. The MC head is asymmetrical in the medial-lateral plane. The articular surface is more extensive on the radial side than on the ulnar side. Therefore, the areas of intra-articular bare bone, which are the preferred sites of erosion in rheumatoid arthritis, are offset and should be examined more proximally on the radial side (Fig. 17). The distribution of cartilage over the MC head varies between the two surfaces. The volar surface is spherical, with a wider cartilaginous articular surface, while the dorsal surface is rough and only the upper portion is covered with cartilage [2]. This distinction is useful in identifying chondropathy and osteochondral lesions in their corresponding anatomical locations. The lateral surfaces of the MC head contain a lateral fossa that ends in a tubercle [2]. The collateral ligament inserts onto this fossa and tubercle [2], which facilitates identification of collateral ligament insertions in imaging. The volar surface of the base of the P1 contains two bony prominences where the VP inserts. These bony landmarks allow for imaging identification of the VP's distal insertions. The joint recess is more developed dorsally [10] and is the preferred site to look for joint effusions in imaging. The normal recess at the base of the dorsal capsule may be mistaken for a ligament tear. A normal synovial recess is present at the distal insertion of the VP [31] and should not be misinterpreted as a VP avulsion on US or MRI. Knowing the position, anatomical insertions, and dorsopalmar course of the proper and accessory CL is essential to assess them in their anatomical plane on imaging and to avoid diagnostic errors. The UCL courses obliquely from a proximal-dorsal position on the MC head to a distal-palmar position on the base of P1 [3–6]. The US probe should be aligned along this oblique path rather than parallel to the longitudinal ulnar axis of the MCPJ. This

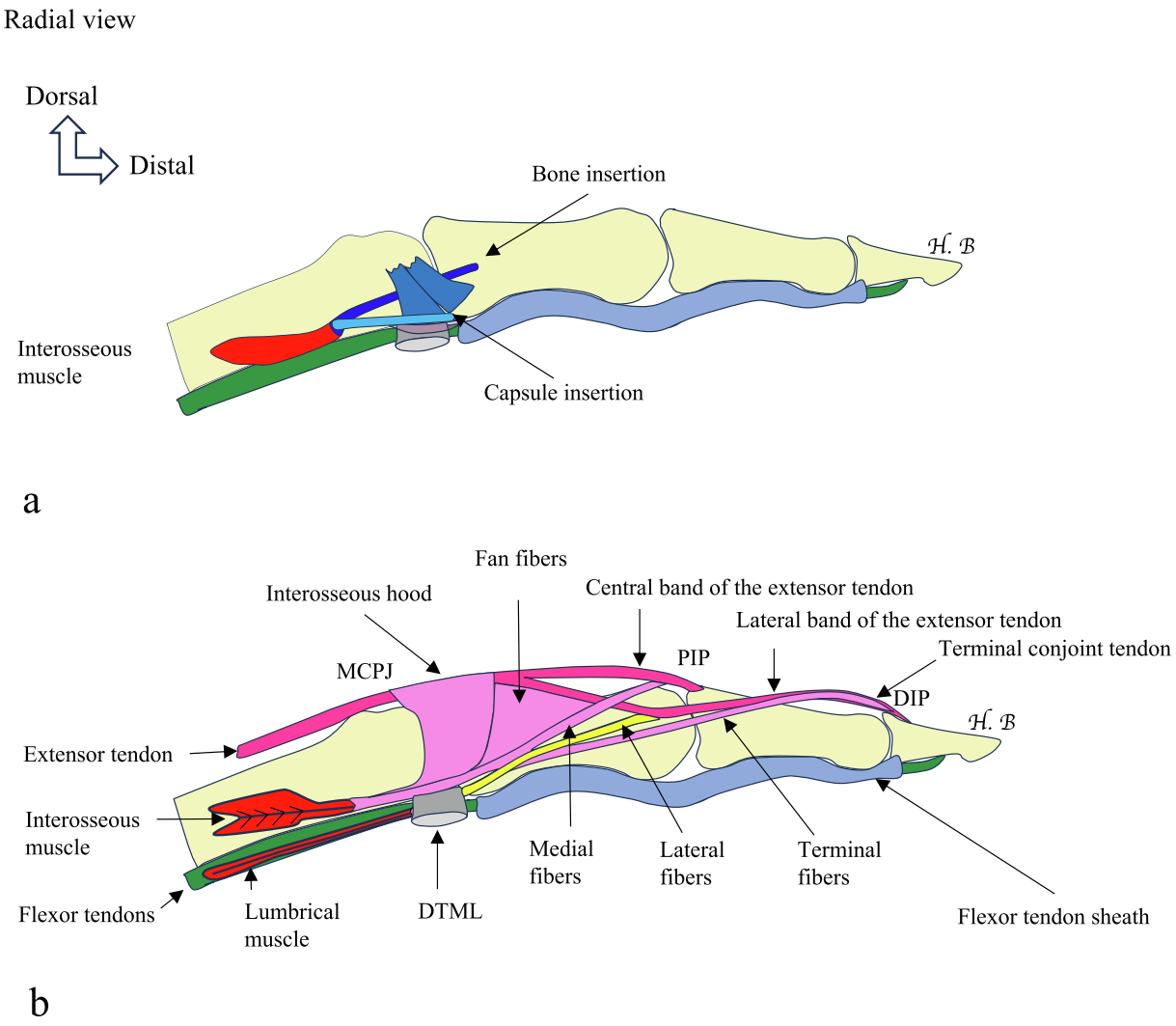

Fig. 12. Schematic illustrations showing the distal insertions of the interosseous muscles. The deep distal insertions of the interosseous muscles (a) are of two types: osseous, attaching to the proximal phalanx, and capsular. The superficial distal insertions (b) attach to the extensor apparatus and are divided into three parts: proximal, middle, and distal. The proximal part is called the interosseous hood. The middle part consists of the fan fibers.The distal part divides into three fiber types: Central fibers, which join the central slip of the extensor tendon to insert on the base of the middle phalanx;Lateral fibers, which merge with the lateral bands of the extensor tendon to form the terminal extensor tendon that inserts on the base of the distal phalanx;Terminal fibers, which blend with the terminal portion of the extensor tendon and insert on the base of distal phalanx.PIP, proximal interphalangeal joint; DIP, distal interphalangeal joint; DTML, Deep transverse metacarpal ligament.

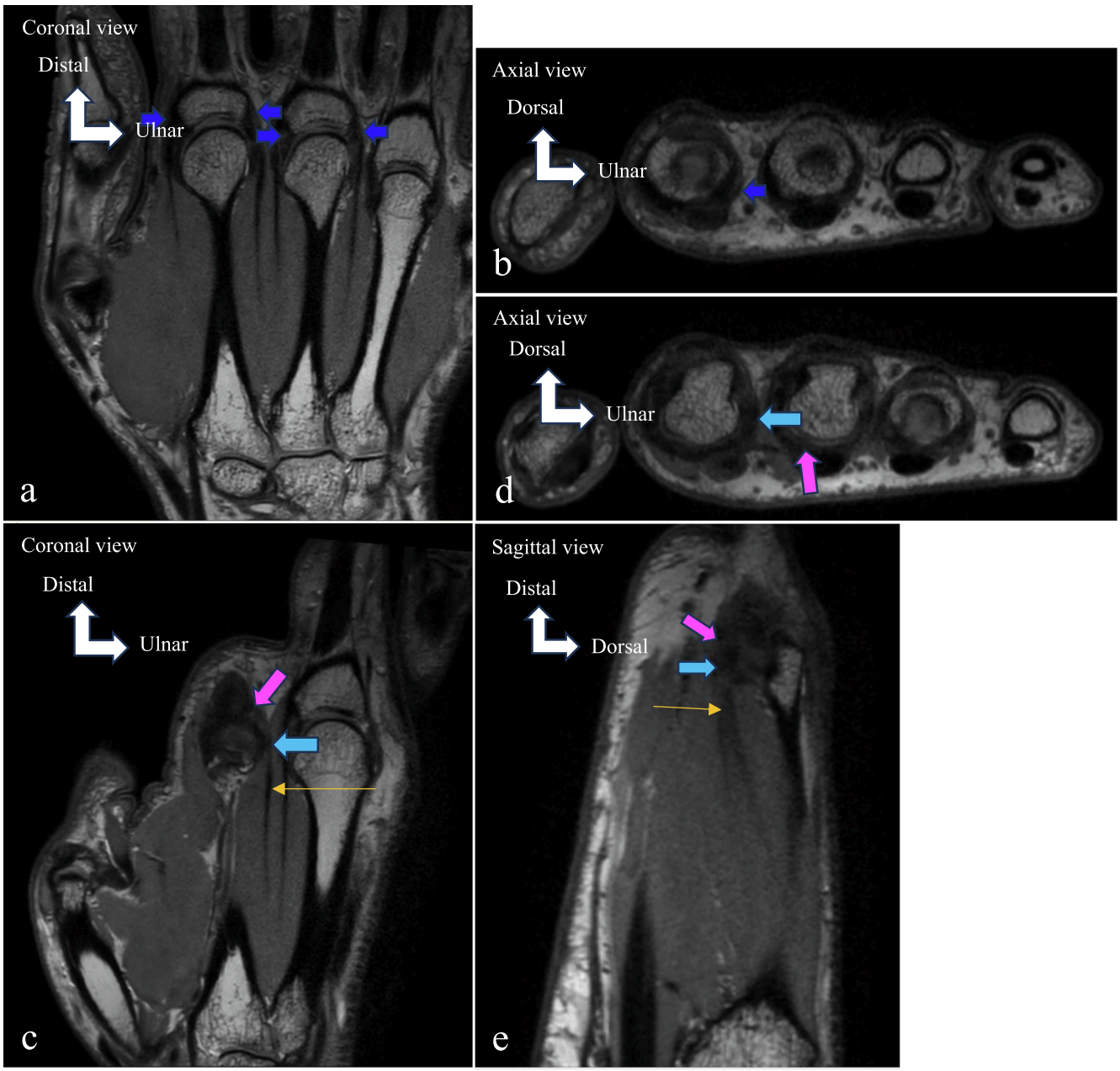

Fig. 13. MRI showing the deep distal insertions of the interosseous muscles. Coronal proton density (PD) MRI (a, c), axial (b, d), and sagittal (e) views. Deep insertion of interosseous muscle tendons on the base of the proximal phalanx (a, b, blue arrows). Deep insertion of the first ventral interosseous muscle tendon on the volar plate (c, d, e, light blue arrows). Volar plate highlighted in pink arrows (c, d, e).

normal path can be misleading on dorsal coronal MRI images, potentially leading to a false-positive diagnosis of distal UCL tear, while the ligament remains intact on more palmar coronal slices at its anatomical insertion. The CL of the MCPJ of the index finger exhibit the greatest sagittal plane obliquity, which decreases progressively toward the ulnar fingers, where the pCL aligns more with the longitudinal axis of P1. This anatomical feature aids in proper imaging evaluation of the CL. Treatment and restoration of RCL stability are particularly important in the MCPJ of the index finger due to the significant forces exerted during pinching, gripping, and tool use [23,32,33]. Each collateral ligament, whether proper or accessory, is composed of three anatomically and functionally distinct parts: dorsal, middle, and palmar [4,6]. Due to its anatomical and biomechanical properties, the MCPJ is significantly more stable in flexion. Therefore, collateral ligament instability tests should be performed with the MCPJ in flexion [13,14]. The pCL is taut in flexion and relaxed in extension [4,5], unlike the accessory ligament [6]. Thus, dynamic US examination is more sensitive when ligaments are evaluated under stress in the appropriate positions. The DTML is a strong fibrous band that maintains the stability of the MC heads and the transverse MC arch. Its integrity is essential for grip strength and the stability of the arch [18]. The SB requires dynamic evaluation in MCPJ flexion and with a clenched fist [22]. The interosseous muscles are intrinsic muscles originating on the MC bones and inserting distally via deep tendons into the VP of the MCPJ and the tubercle of the P1 base, and superficially into various components of the extensor mechanism. Their functions include MCPJ flexion, abduction/adduction, and extension of the proximal and distal interphalangeal joints. Intrinsic muscle paralysis, leading to a claw deformity (MCPJ hyperextension and interphalangeal joint flexion), occurs in fingers where extrinsic muscles are functional. In contrast, intrinsic paralysis without a claw deformity is

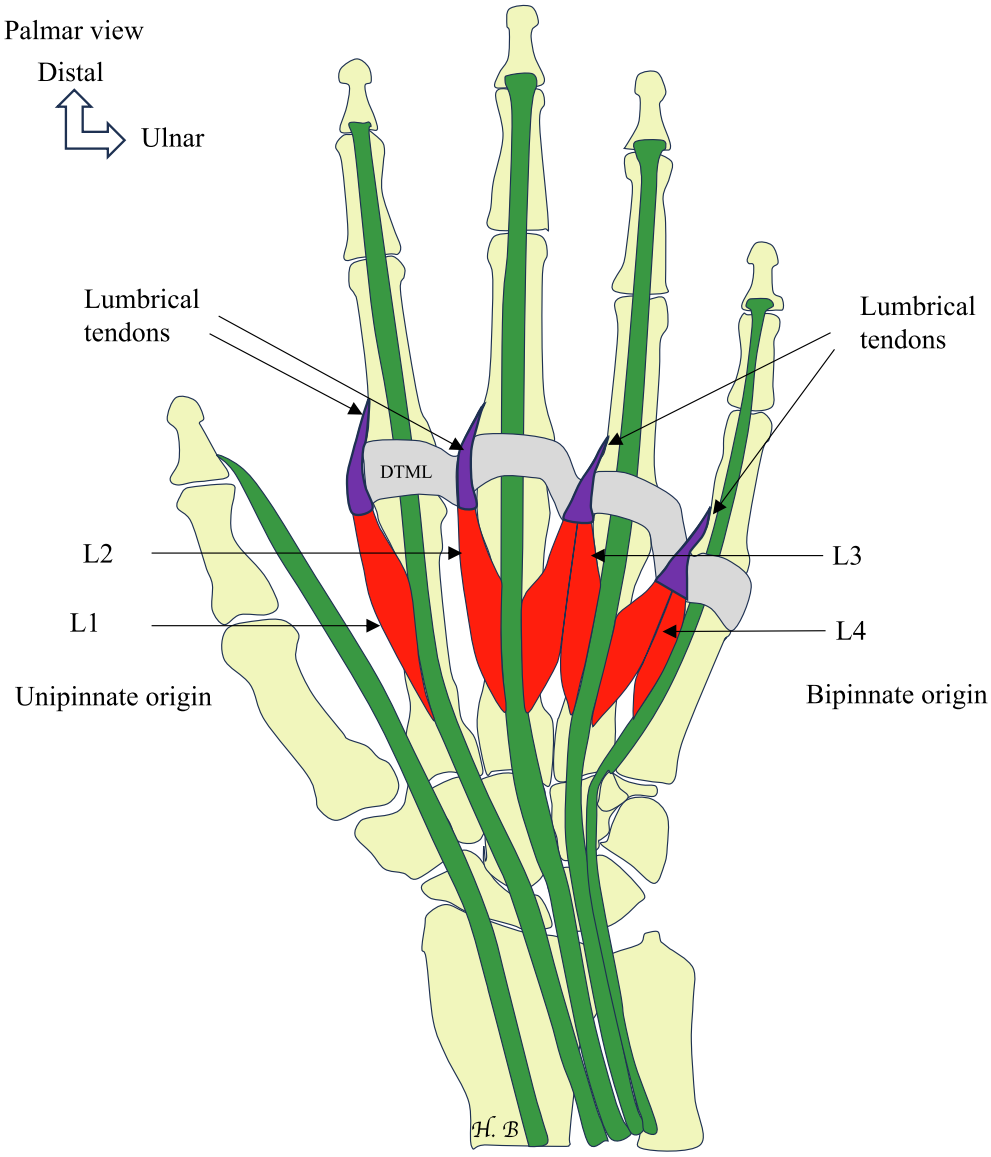

Fig. 14. Schematic illustration showing the lumbrical muscles. L1: First lumbrical muscle; L2: Second lumbrical muscle; L3: Third lumbrical muscle; L4: Fourth lumbrical muscle; DTML: Deep transverse metacarpal ligament.

due to extrinsic muscle impairment (either laceration or paralysis) [34]. The "Zancolli assembly core" is a fibrous continuum made up of fibers from the VP, SB, CL, A1, and DTML [7,8]. Recognizing this structure in imaging allows the identification of associated lesions.

4. Imaging of the MCPJ of the long fingers

Lesions of the MCPJ of the fingers require precise diagnosis, as the loss of function in even a single MCPJ can significantly impair overall hand function [35]. To ensure appropriate treatment, accurate identification of the damaged anatomical structures is essential. Several imaging modalities are used in addition to standard radiographs to evaluate MCPJ injuries. Dynamic conventional radiography can assess MCPJ instability and may indirectly suggest ligamentous injury [36]. MCP arthrography has also been employed to detect collateral ligament injuries [37]. US is well suited for imaging the fingers, but access to the intermetacarpophalangeal spaces may be technically limited due to the presence of adjacent digits. MRI plays a crucial role in evaluating MCPJ abnormalities. Recent advances in MRI technology have enhanced the assessment of both intra- and periarticular structures, offering excellent spatial resolution and soft-tissue contrast—both essential for precise anatomical analysis of the MCPJ [38–40].

4.1. Imaging Modalities in Clinical Practice

The choice of imaging technique for the MCPJ should be guided by clinical symptoms, the anatomical structures to be examined, and the pathological context. Conventional radiography is the first step. It is indicated in osteoarthritis [41]. It is indicated in the initial assessment of trauma, to look for fractures or dislocations. It is also used at the initial stage and for monitoring rheumatic diseases such as rheumatoid arthritis, psoriatic arthritis, or systemic sclerosis [42]. It allows detection of bone erosions and arthropathies. In suspected microcrystalline arthritis due to calcium pyrophosphate dihydrate deposition disease, it helps identify joint calcifications. Dynamic fluoroscopic radiography is used to assess joint instability.

US is a non-invasive, dynamic, and accessible modality, particularly suited for exploring superficial structures such as the SB, CL, VP, pulleys, and tendons. It allows comparative analysis with the contralateral side and is highly effective in trauma settings for assessing ligamentous,

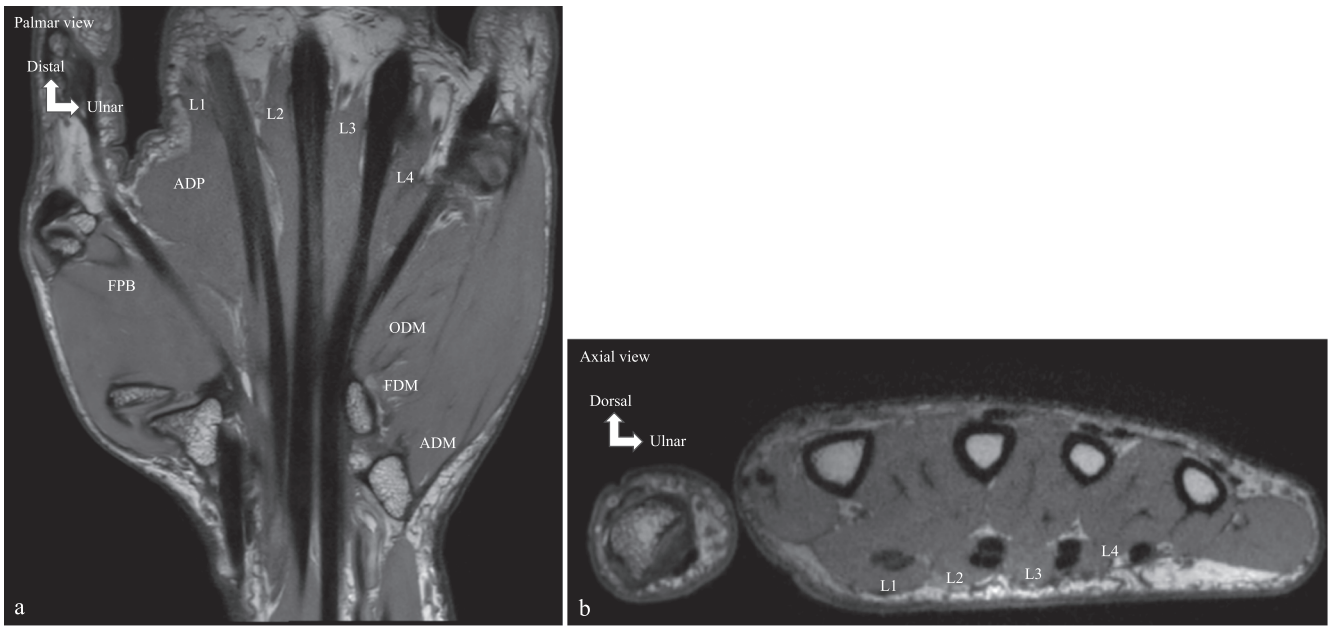

Fig. 15. MRI showing the lumbrical muscles. Coronal (a) and axial (b) proton density (PD) MRI sequences. L1: First lumbrical muscle; L2: Second lumbrical muscle; L3: Third lumbrical muscle; L4: Fourth lumbrical muscle; FPB: Flexor pollicis brevis; ADP: Adductor pollicis; FDM: Flexor digiti minimi; ODM: Opponens digiti minimi; ADM: Abductor digiti minimi.

tendinous, or capsular lesions. However, some areas, notably the intermetacarpal spaces, remain difficult to access, limiting its effectiveness for complete exploration of CL. In inflammatory pathologies, especially rheumatoid arthritis, it offers excellent sensitivity for detecting early synovitis and joint effusions [42,43]. It also allows analysis of the interosseous and lumbrical muscles, initial assessment of soft tissue masses, as well as evaluation of MCPJ locking. Moreover, US facilitates guided interventional procedures, such as percutaneous biopsies or therapeutic infiltrations.

CT scanning is indicated for the assessment of complex fractures or dislocations, as well as for analysis of bone texture in the evaluation of bone tumors. CBCT, used in our institution, offers higher spatial resolution than conventional CT for bone study. It is particularly suited to analysis of cortices, erosions, fracture lines, and calcifications.

MRI is currently the reference technique for detailed analysis of intra- and periarticular structures [42,43]. It allows evaluation of bones, tendons, pulleys, ligaments, and cartilage. It is particularly indicated when ligamentous injuries are suspected, especially those inaccessible to US in the intermetacarpal spaces or in early inflammatory pathologies. MRI, due to its excellent tissue resolution, is essential when clinical suspicion concerns deep ligamentous lesions, early erosions, or subtle cartilage or marrow changes, in accordance with EULAR recommendations in rheumatoid arthritis [42]. MRI is the best modality for diagnosing avascular necrosis of the MC head [44].

4.2. Radiographs of the MCPJ of the long fingers

Radiographic evaluation must be rigorous and, in case of any doubt, should be supplemented with additional views.

4.2.1. Posteroanterior view of the MCPJ

The posteroanterior view is the standard baseline projection. The palm is placed flat on the imaging table, the X-ray beam is directed vertically and centered on the head of the third MC, with the fingers extended and slightly separated (Fig. 18, a). On the radiograph, the fingers should appear separated, with no overlap or rotation, as confirmed by the symmetrical appearance of the ulnar and radial concavities of the P1. The joint spaces should be clearly visible (Fig. 18, d).

4.2.2. Brewerton view for MCP head assessment [45].

This view is useful for detecting erosions of the MC heads, from the second to the fifth MCP joints. The dorsal surfaces of the fingers are placed flat against the image receptor, with MCP joints flexed between 45° and 65°. The thumb remains in extension. The X-ray beam is angled 15° to 20° toward the radial side and centered on the third MC head (Fig. 18, b, e).

4.2.3. Oblique posteroanterior views in semipronation and semisupination

Oblique radiographic views are useful for optimal visualization of the MCP joints (Fig. 18, c, f), particularly due to the natural arch formed by the metacarpals in the axial plane.

4.2.4. Lateral view of the MCPJ

The X-ray beam is centered directly on the MCPJ.

4.3. Normal CT Scan and Cone-Beam CT (CBCT) of the MCPJ of the long fingers

CT scanning provides the highest resolution for evaluating bone architecture, allowing precise assessment of erosions, calcifications, cortical bone, and fracture lines. In our institution, we exclusively use CBCT (Fig. 19) instead of conventional CT. CBCT is a 3D imaging technique specifically suited for peripheral joints, offering excellent spatial resolution—superior to that of conventional CT—and enables multiplanar reconstruction.

4.4. Ultrasound of the MCPJ of the long fingers

Anatomical knowledge is essential to performing high-quality US of the MCPJ (Fig. 20). A hockey stick-shaped transducer is used for optimal access. Comparison with adjacent asymptomatic MCPJ and the contralateral hand is recommended. The SB (Fig. 21, e, f) are evaluated in short-axis views. The radial and ulnar SB extend both superficially and

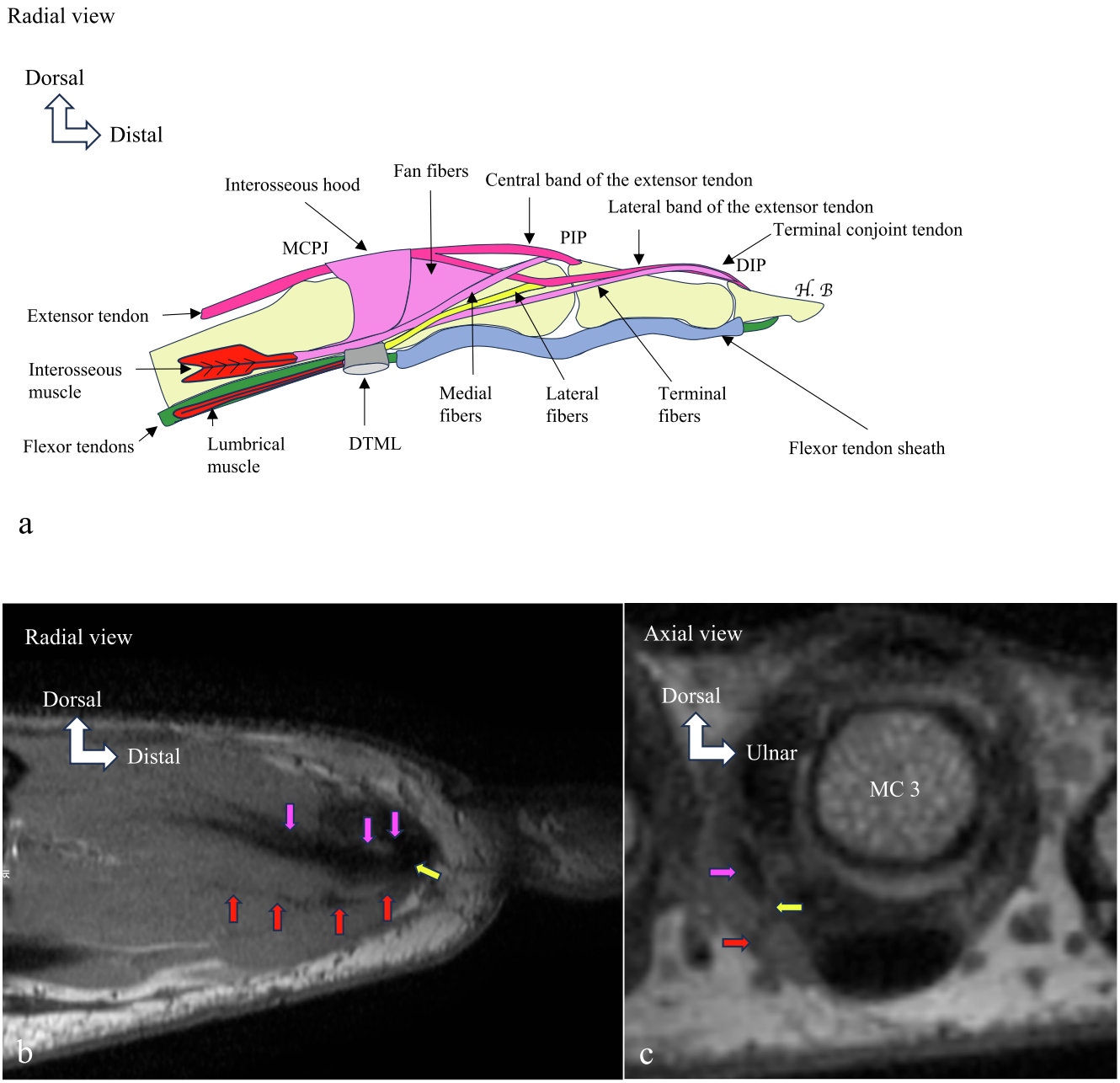

Fig. 16. Schematic illustration and MRI showing the connection between the interosseous tendon and the lumbrical tendon (a). Radial and axial proton density (PD) MRI views (b, c) of the third MCPJ. Medial fibers of the interosseous tendon (pink arrows); lumbrical tendon (red arrows); fusion between the two tendons (yellow arrow).

deeply, attaching to the respective sides of the ET. On US, they appear thin, regular, homogeneous, and hypoechoic [46]. Their thickness ranges from 0.42 to 0.72 mm, with no significant differences between digits 2 to 5 or between dominant and non-dominant hands [46,47]. US can evaluate the alignment of the ET relative to the dorsal surface of the MC head and detect radial or ulnar subluxation/dislocation, as well as SB tears. Dynamic imaging during flexion and extension with the hand in a fist position is essential for a comprehensive evaluation. The palmar extensions of the SB and their insertions into the DTML and the VP can also be assessed. Within the intermetacarpal space, however, evaluation of the SB may be technically limited due to transducer access constraints [46]. Among the CL (Fig. 21, g), only the RCL of the index MCPJ and the UCL of the fifth MCPJ can be reliably assessed with US. These are thick, fibrillar, echogenic structures located in grooves on the respective radial and ulnar aspects of the second and fifth MC heads, extending distally to the base of the P1. These grooves are clearly visible in coronal US images and serve as useful osseous landmarks for locating the proximal attachment of the CL. Differentiation between the pCL and aCL remains challenging on US. Sesamoid bones (Fig. 21, k) may be present on the palmar side—typically on the radial aspect of the second MC head and the ulnar aspect of the fifth. A bipartite sesamoid bone may occasionally be observed. These sesamoids are embedded within the VP. The dorsal MC synovial recess (Fig. 21, d) is the most prominent and consistently visible on US, appearing as an echogenic band beneath the deep surface of the ET. A small osseous depression may be seen on the dorsal aspect of the second, third, or fifth MC heads—corresponding to a bare area between the articular cartilage and the dorsal capsular insertion—while this is typically absent on the fourth. The articular cartilage of the MC

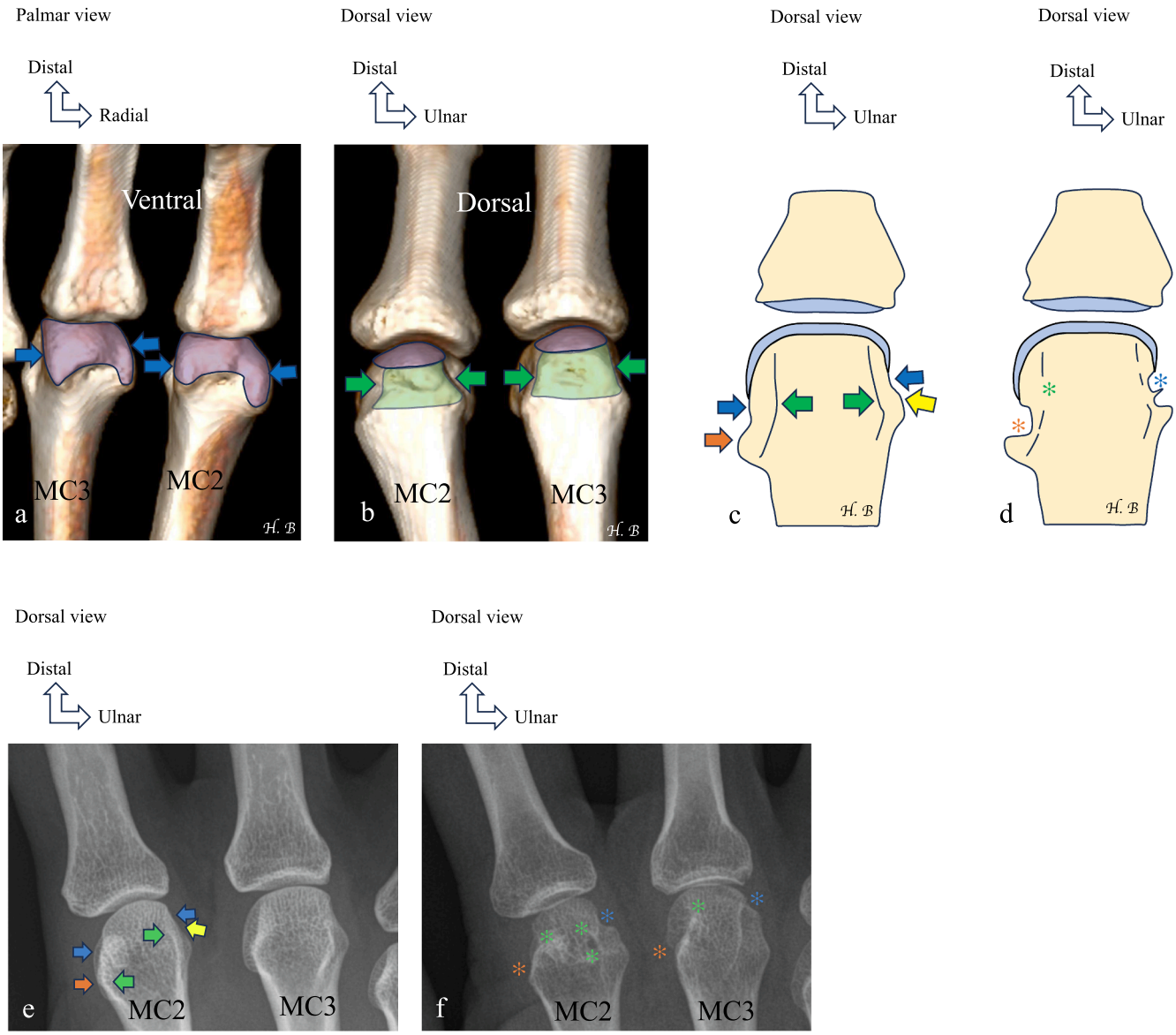

Fig. 17. Normal and eroded metacarpal heads. Volume rendering reconstructions (a, b), schematic drawings (c, d), posteroanterior radiographs (e, f). It is important to understand the anatomy of the metacarpal head:Its volar (palmar) aspect is marked by two bony prominences on the ulnar and radial borders, which are slightly convex (a, c, blue arrows), whereas its dorsal aspect is delineated by two sharper, slightly concave lateral ridges (b, c, green arrows).In the assessment of erosive arthropathies, such as rheumatoid arthritis, erosions typically occur on these prominences and ridges (d).In addition, the metacarpal head is asymmetrical in the medial-lateral plane: the radial articular surface is more extensive longitudinally (c, orange arrow) than the ulnar surface (c, yellow arrow).Erosions in rheumatoid arthritis tend to occur in bare intra-articular bone zones, which are asymmetrically positioned and therefore should be specifically examined more proximally on the radial aspect (d).(e) Normal appearance: volar bony prominences (e, blue arrows), dorsal ridges (e, green arrows), radial articular surface (e, orange arrow), ulnar articular surface (e, yellow arrow). (f) Marginal erosions of the volar aspects with loss of dorsal ridges (green asterisks) and volar prominences (blue asterisks) of MC2 and MC3 in a 40-year-old patient with rheumatoid arthritis. Proximal radial erosions of the volar bony prominences (orange asterisks).MC2, second metacarpal; MC3, third metacarpal.

head and the base of P1 appears as a thin hypoechoic layer on US (Fig. 21, d, f, h). The triangular dorsal fibrocartilage of the MCPJ (also known as the dorsal plate) (Fig. 21, d) is a slightly echogenic, homogeneous structure interposed between the MC head and the base of P1, deep to the ET. It has a triangular appearance on sagittal imaging [48]. The VP (Fig. 21, h, i, j, k) lies deep to the flexor tendons. Its assessment requires both long- and short-axis imaging. It is homogeneously echogenic on US [48]. Degenerative changes or tears appear as hypoechoic gaps, particularly near the insertion on P1. The A1 (Fig. 21, j) is seen on transverse palmar views as a thin, ring-like structure superficial to the FT and inserting into the VP. The DTML (Fig. 21, i) is assessed in the transverse plane. Dynamic US with finger abduction is helpful for evaluating its integrity. It appears as a uniformly echogenic and thick structure between adjacent MCP joints. The interosseous muscles are located dorsally and deep to the lumbricals and DTML. The lumbrical muscles, common palmar digital nerves, and vessels lie on the palmar side of the DTML and are identifiable on US (Fig. 21, i).

4.5. *MRI of the MCPJ of the long fingers*

MRI is an excellent modality for analyzing the MCP joints [38,39]. MRI of the fingers should be performed on high-field MRI machines (at

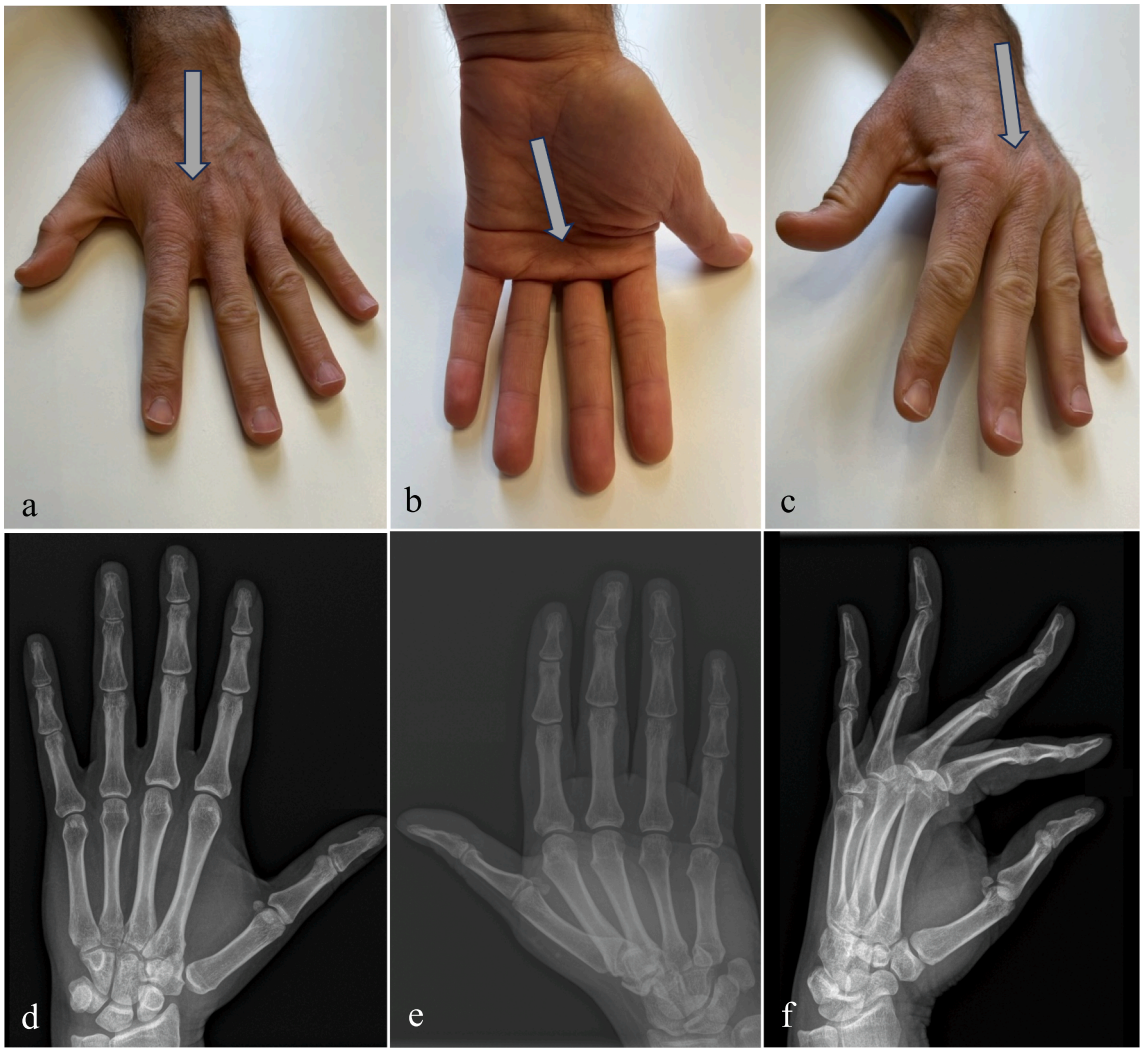

Fig. 18. Standard radiographs of the MCP joints of the long fingers. Posteroanterior view (a, d), Brewerton view (b, e), oblique posteroanterior view in semi-pronation (c, f).

least 1.5 T, but preferably a 3 T magnet), with dedicated multichannel coils. MRI is a precise imaging technique for evaluating abnormalities of bones, tendons, pulleys, ligaments, cartilage, and synovium. The patient should be positioned in the "Superman position" with the arm extended above the head. This positioning allows alignment of the region of interest at the scanner isocenter. However, this position can be uncomfortable and difficult to maintain, potentially causing motion artifacts. If the patient is not too large and the previous positioning is not tolerated, the hand can be scanned with the patient supine and the arm alongside the body.

Bone structures, fractures, and avulsions related to ligament or VP injuries are best assessed with T1-weighted images. Detection of bone marrow edema and soft tissue lesions (CL, extensor hood, SB, DTML, muscles, tendons, pulleys, synovium) is optimally performed using T2-weighted images with fat suppression (FS) or STIR sequences. A T1-weighted image and fluid-sensitive sequences in three orthogonal planes should be included in the basic imaging protocol (Table 1: Suggested MRI protocol by the ESSR Sports Sub-committee). MR imaging and MR arthrography allow diagnosis of MCPJ lesions (Fig. 22). MR arthrography does not offer a significant advantage over conventional MRI [39]. The only advantage of MR arthrography compared to conventional MRI is better visualization of the cartilage surface (Fig. 22) [49]. When MR arthrography is performed, in addition to cartilage assessment, it is used to detect collateral ligament tears (contrast leakage at the tear site) [37], VP ruptures (contrast leakage into the flexor tendon sheath) [50], and capsular ruptures (contrast leakage) [24]. The sensitivity for detecting lesions of the pCL, aCL, and the A1 is high. Sensitivity is slightly lower for detecting extensor hood structures, the DTML, and the VP [39]. The proximal and distal attachments of the pCL are well visualized on MRI (Fig. 23). The proximal attachments of the aCL are not separable from those of the pCL. The aCL insert distally on the VP. The thickness of the RCL is slightly greater than that of the UCL. The SB are studied in the transverse plane during maximal flexion and extension to assess for any subluxation or dislocation of the ET (Fig. 24). The transverse fibers of the extensor hood (Fig. 25), the fibrous connections of the extensor hood linking the intrinsic and extrinsic extensor tendons, the DTML, and the interosseous and lumbrical muscles and tendons are best analyzed in the transverse plane (Fig. 26). The sagittal plane is optimal for visualizing the VP and joint recesses.

Among the limitations of this review, it must be noted that the analysis is based on our personal experience and the institutional workflow for managing MCPJ disorders of the long fingers. Due to the small size and confluent insertions of certain anatomical structures, some components remain only partially visualized, even with the use of

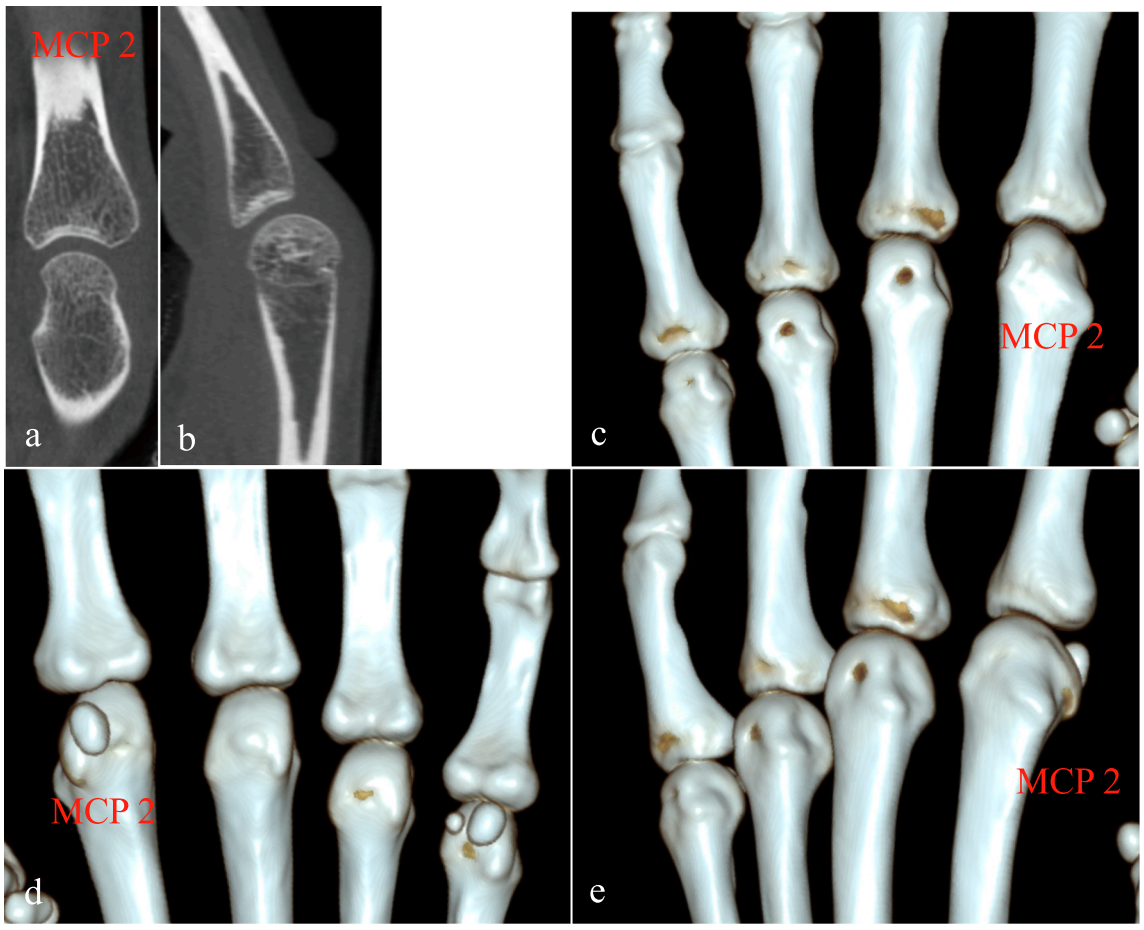

Fig. 19. CBCT of the index MCPJ. Coronal view (a), sagittal view (b). CBCT volume rendering reconstructions : dorsal view (c), palmar view (d), oblique view (e).

high-field 3T MRI. A more detailed evaluation would likely require enhanced spatial resolution and tissue contrast — particularly to differentiate the individual bundles of the proper and accessory collateral ligaments, the superficial and deep layers of the sagittal band, the insertions and interconnections of the interosseous and lumbrical muscles, and the multiple components of the so-called "Zancolli's assembly core" (Fig. 26). Additionally, this study did not assess interindividual variability in the ligamentous, osseous, and musculo-tendinous structures through imaging or cadaveric dissection.

4.6. Recent Advances in MCPJ Imaging

Imaging of the MCPJ of the long fingers has significantly advanced in recent years due to technological progress across multiple modalities: digital radiography, CT, US, and MRI. These tools now play a crucial role in the diagnosis and monitoring of joint pathologies. Digital radiography remains the gold standard for evaluating and following bone lesions, especially in inflammatory arthritides such as rheumatoid arthritis and degenerative joint diseases. Advances in artificial intelligence have enabled automated scoring of radiographic lesions, improving diagnostic accuracy and consistency [51]. Moreover, deep learning algorithms are employed to automatically detect calcium pyrophosphate crystal deposits, aiding in the diagnosis of chondrocalcinosis [52], as well as to classify and quantify the severity of hand osteoarthritis [53]. High-resolution peripheral quantitative computed tomography (HR-pQCT) has emerged as a powerful tool for detailed three-dimensional assessment of MCPJ, allowing precise measurement of volumetric bone mineral density, joint space, and erosion volumes with fine isotropic resolution. Fully automated segmentation methods for quantifying bone mineral density in MC bones have been demonstrated [54], and consensus approaches for 3D joint space width quantification have been proposed [55]. HR-pQCT is well tolerated in clinical practice and delivers high-quality images even during active inflammation [56]. Other advanced CT modalities, such as dual-energy CT (DECT) with iodine mapping and contrast-enhanced CT, show performance comparable to MRI in detecting inflammatory changes, particularly in psoriatic arthritis of the hands [57,58]. High-resolution US has become indispensable for evaluating inflammatory and functional aspects of MCPJ. It enables real-time detection of early, even subclinical abnormalities, particularly in systemic sclerosis [59]. Artificial intelligence integration, particularly through convolutional neural networks, improves cartilage thickness measurement and automates synovial proliferation detection, enhancing diagnostic objectivity and efficiency [60,61]. Generative high-resolution models (HRGANs) further compensate for limited annotated datasets, enhancing algorithm performance [62]. These advancements confirm the complementary role of US alongside MRI in clinical workflows [63]. MRI remains the reference modality for comprehensive assessment of the bony, cartilaginous, ligamentous, and synovial structures of MCPJ. Use of dedicated 3 Tesla coils markedly improves resolution and diagnostic quality. Accurate interpretation requires thorough anatomical knowledge [64]. Complex cases such as synovial chondromatosis with atypical MRI findings demand multidisciplinary management [65]. Among recent innovations, zero echo time (ZTE) MRI offers a promising approach for bone imaging. This technique visualizes cortical and trabecular bone with contrast resembling radiography or CT, by rapidly acquiring signals from tissues with extremely

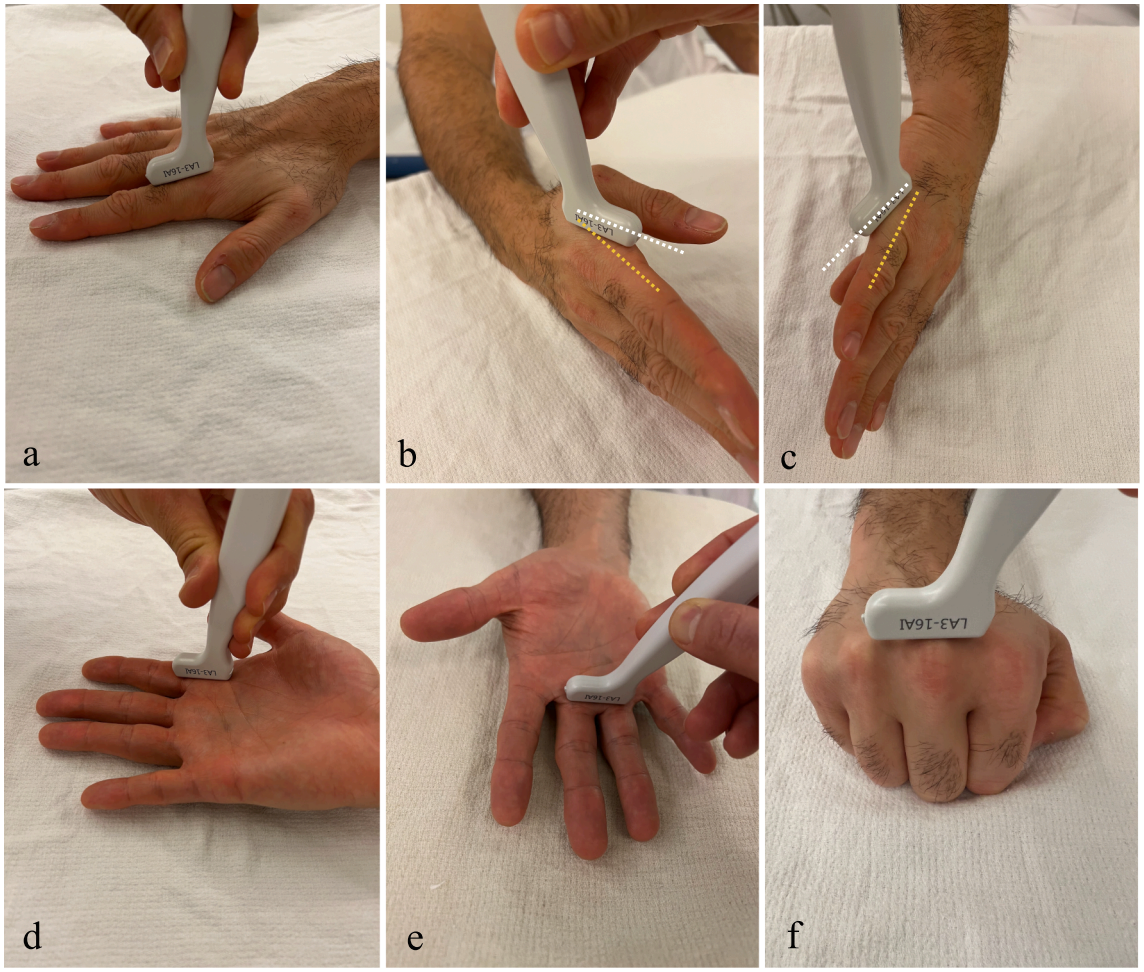

Fig. 20. Ultrasound technique for evaluating the MCPJ of the long fingers. *Longitudinal dorsal US of the index MCPJ (a):* The probe is positioned along the longitudinal axis of the MCPJ with the finger in extension. *US of the radial collateral ligament of the index MCPJ (b):* The radial collateral ligament originates dorsally from the metacarpal and inserts distally and palmarly onto the P1. The US probe should follow this dorsopalmar oblique path (white line) rather than the radial longitudinal axis of the MCPJ (orange line). The ligament is examined in the coronal plane along the radial aspect of the MCPJ, where it appears as a continuous fibrillar structure. *US of the lateral collateral ligament of the index MCPJ (c):* The lateral collateral ligament originates dorsally from the metacarpal and inserts distally and palmarly onto P1. The probe must be aligned along the dorsopalmar oblique path (white line) and not parallel to the ulnar longitudinal axis of the MCPJ (orange line). The ligament is assessed in the coronal plane along the ulnar side of the MCPJ. *Palmar US of the index MCPJ (d):* The probe is placed along the longitudinal axis of the MCPJ with the finger in extension. *Palmar US of the intermetacarpal space (e):* The probe is positioned transversely (axial view) across the intermetacarpal space with the fingers extended. *Dorsal US of the MCPJ (f):* The probe is positioned in the axial plane over the dorsal surface of the MCPJ. The extensor tendons should be assessed dynamically during finger flexion and with the hand in a clenched fist position.

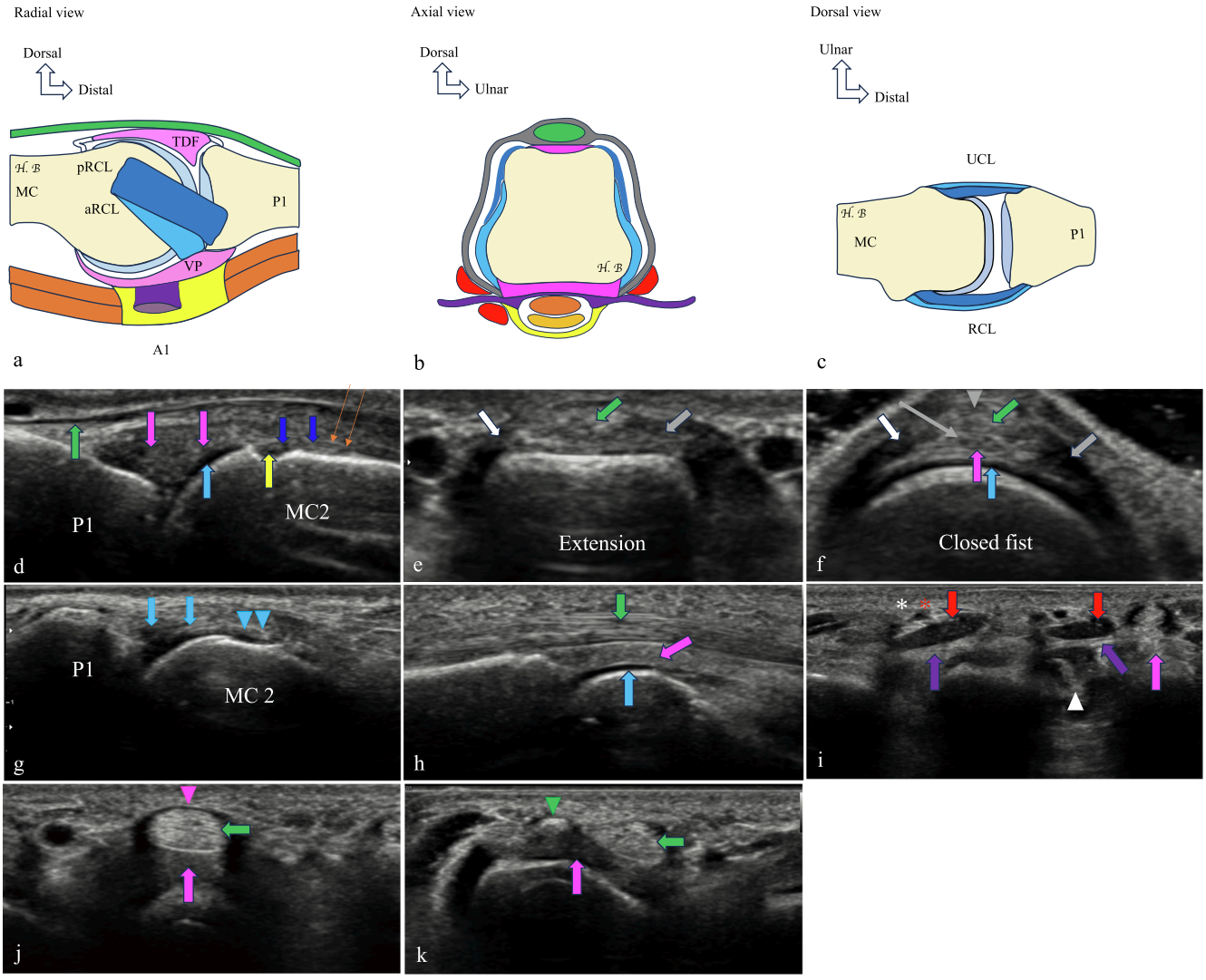

Fig. 21. Ultrasound features of the MCPJ of the long fingers. Schematic drawings (a, b, c). Ultrasound images (d, e, f, g, h, i, j, k). *Longitudinal dorsal US of the index MCPJ (a, d):* The dorsal metacarpal synovial recess appears as an echogenic band (dark blue arrows, d) with a tapered proximal border (thin orange arrows, d). The triangular dorsal fibrocartilage displays a truncated, pointed configuration interposed between the metacarpal head and the base of the proximal phalanx (pink arrow, d). A small depression (yellow arrow, d) on the dorsal aspect of the second metacarpal head corresponds to a bare area between the cartilage and the dorsal capsular insertion. Articular cartilage (light blue arrow, d), extensor tendon (green arrow, d). *Transverse dorsal US of the index MCPJ (e, f):*Short-axis sonographic view of the dorsal aspect of a normal MCPJ. The sagittal band is visualized in both its superficial and deep components at the midline, with the deep portion located superficial to the dorsal plate and the articular cartilage of the metacarpal head. Radial sagittal band (grey arrow, e, f) Ulnar sagittal band (white arrow, e, f) Deep portion of the sagittal band (long thin grey arrow, f) Superficial midline portion (grey arrowhead, f) Extensor tendon (green arrow, e, f), triangular dorsal fibrocartilage (pink arrow, f), articular cartilage (blue arrow, f). *Coronal US of the radial aspect of the index MCPJ (g):* Radial collateral ligament (light blue arrows, g), inserting into a depression on the metacarpal head (light blue arrowheads, g). *Palmar US of the index and middle MCPJs (h, i, j, k):* Long-axis image (h) shows hypoechoic articular cartilage (light blue arrow, h) and triangular dorsal fibrocartilage (pink arrow, h). The volar plate is evaluated using both short-axis (pink arrow, i, j) and long-axis (pink arrow, k) views. It appears as a homogeneously echogenic structure. Degenerative changes or tears in the volar plate present as hypoechoic gaps or defects, particularly near its insertion on the proximal phalanx. Sesamoid bones may occasionally be seen on the palmar side: radially on the second metacarpal head (green arrowhead, k) and ulnarly on the fifth. Bipartite sesamoids can also be observed. These bones are embedded within the volar plate. *The deep transverse metacarpal ligament (DTML)* (purple arrow, i) is evaluated in the transverse plane. It shows uniform echogenicity and thickness across the intermetacarpal spaces. Dynamic ultrasound with finger abduction helps assess DTML integrity. *Lumbrical muscles* (red arrows, i), *nerves* (white asterisk, i), and *common palmar digital vessels* (red asterisk, i) are evaluated on the palmar side of the DTML using ultrasound. *Interosseous muscles* (white arrowhead, i) are located dorsally and deeper relative to the lumbricals and the DTML. *Flexor digitorum superficialis and Flexor digitorum profundus tendons* (green arrows, h, j, k) and the *A1 pulley* (pink arrowhead, j) are also visualized.

Table 1
Basic sample protocol for MRI of fingers suggested by the ESSR sports subcommittee (https://essr.org/content-essr/uploads/2016/10/ESSR-MRI-Protocols-Fingers.pdf).

	FOV	Slice	TE	Matrix (min.)
Ax PD FS	8 x 10 cm	3 – 3,5 mm	25 – 35	210 x 320
Ax T1	7 x 10 cm	3 – 3,5 mm	min.	260 x 320
Cor PD FS	10 x 12 cm	2 mm	25 – 35	210 x 384
Sag PD FS	10 x 12 cm	2 mm	35 – 45	210 x 384
Cor STIR	10 x 12 cm	2 – 2,5 mm	35 – 45	180 x 320

FOV: field of view, FS: fat-suppressed, PD: proton density, STIR: short tau inversion recovery, TE: echo time.

short T2 relaxation times and low proton density. However, soft tissue contrast is reduced due to proton density weighting and grayscale inversion commonly applied in this sequence. ZTE provides isotropic or near-isotropic 3D acquisitions but remains limited by spatial resolution inferior to conventional imaging and requires complex post-processing for volumetric reconstructions. Optimization involves tuning bandwidth, flip angle, field of view, and matrix size. This modality proves useful for detecting various musculoskeletal conditions, including fractures, loose bodies, erosions, calcifications, bone tumors, and morphometric bone analyses that aid diagnosis and treatment monitoring [66]. Ultra-high field 7 Tesla MRI provides near 200-micron isotropic spatial resolution, enabling fine visualization of joint tissues and early detection of cartilage alterations via T2 mapping [67,68]. Furthermore, dynamic contrast-enhanced MRI (DCE-MRI) combined with AI quantification

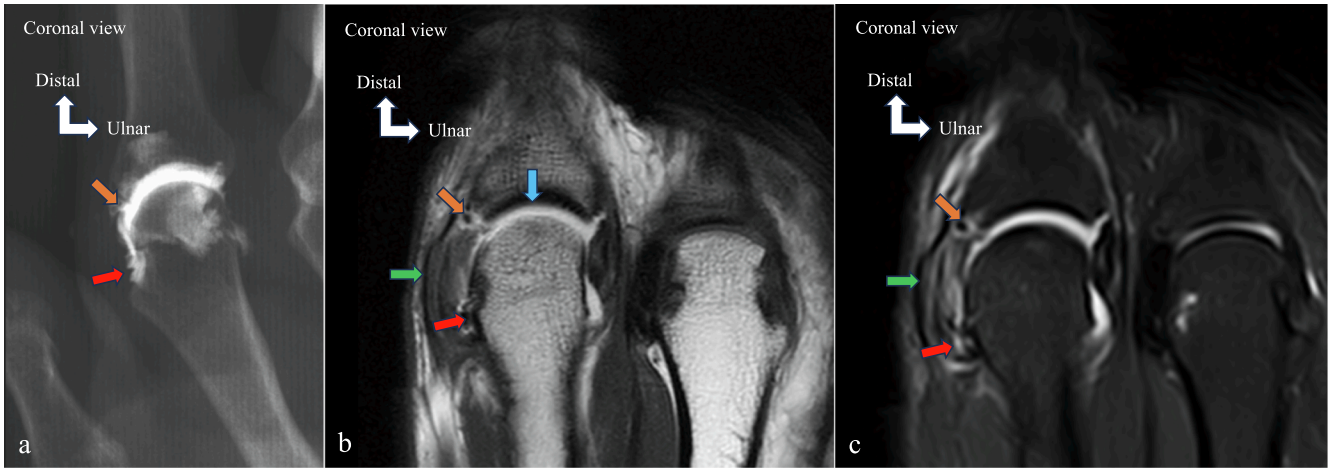

Fig. 22. MR Arthrography of the index finger MCPJ in extension. Frontal arthrography of the index MCPJ (a). Coronal T1 MR arthrography of the index MCPJ in extension (b) and coronal proton density fat-suppressed (PD FS) MR arthrography in extension (c). Rupture of the radial collateral ligament (RCL) and avulsion of the RCL proximal attachment at P1 (orange arrow, a, b, c). Thickening of the RCL (green arrow, b, c). Deep fissuring of the metacarpal attachment of the RCL (red arrow, a, b, c). Well-visualized cartilage (blue arrow, b).

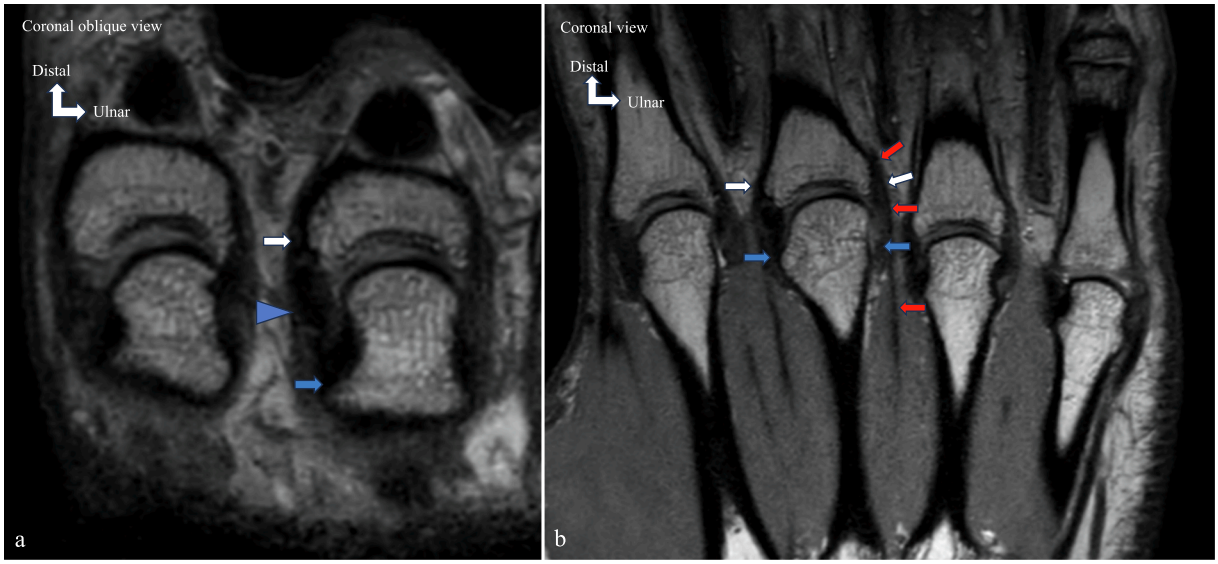

Fig. 23. Collateral ligament and interosseous tendon. Proton density (PD) MRI in oblique dorsopalmar coronal reconstruction of the middle finger MCPJ (a) and coronal plane (b). Proximal attachments (blue arrows, a, b), distal attachments (white arrows, a, b), and body (arrowhead, a) of the proper collateral ligament. The interosseous tendon (red arrows, b) is clearly visualized.

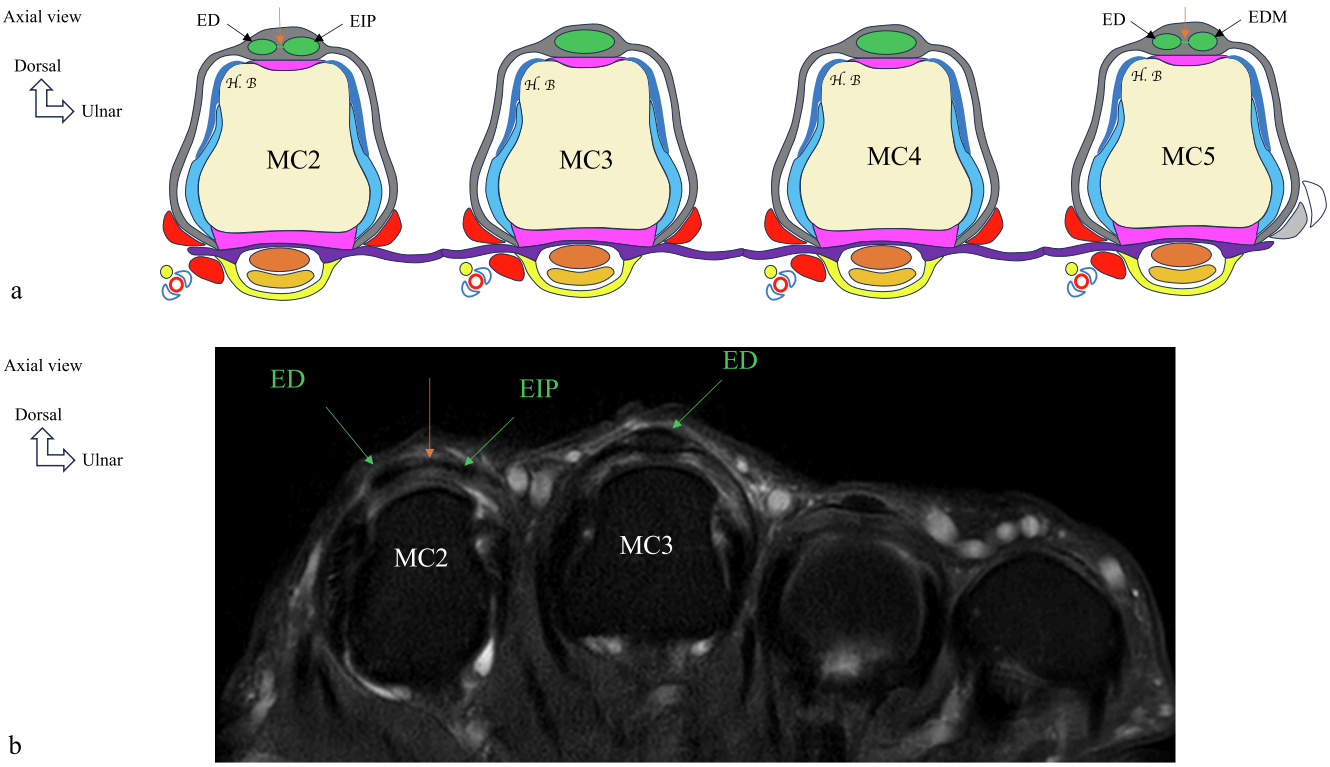

Fig. 24. MCPJ in flexion. Schematic drawing (a). Axial proton density fat-suppressed (PD FS) MRI of the MCPJ in flexion.The sagittal bands are evaluated in the transverse plane during flexion to demonstrate any subluxation or dislocation of the extensor tendons (ET). *Schematic drawing:* The ulnar relationship of the EIP EDM tendons, when present (on the dorsal aspects) of the 2nd or 5th digits, is shown in relation to the ED tendons. An interconnection band between two tendons (in the 2nd or 5th finger) is depicted (orange arrow, a, b). In the 3rd and 4th digits, only a single ED tendon is present. *MRI of the dorsal MCPJ in flexion:* Two extensor tendons (ED and EIP) are visible within the sagittal bands covering the 2nd MCPJ. A single ED tendon covers the dorsal aspect of the 3rd MCPJ (the 4th MCPJ appears similarly). ED, extensor digitorum; EDM, extensor digiti minimi; EIP, extensor indicis proprius.

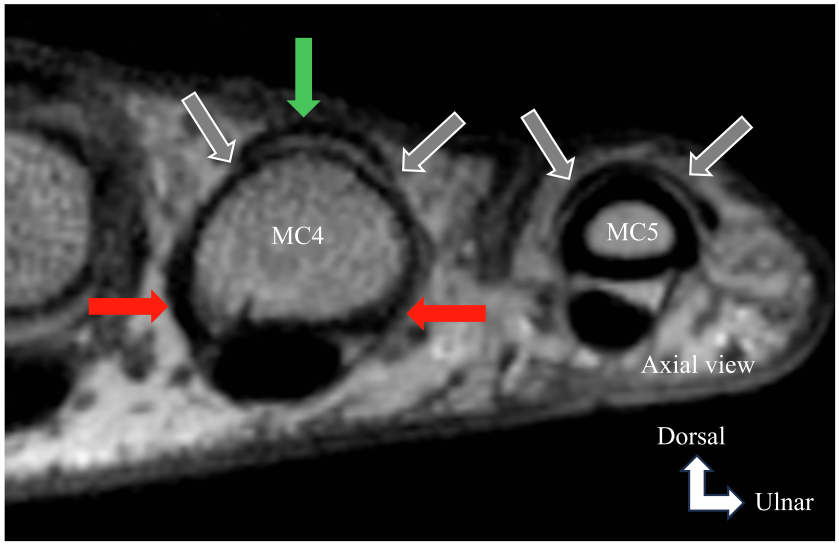

Fig. 25. Axial proton density (PD)–weighted MRI of the MCPJ of the fourth and fifth fingers showing transverse fibers (gray arrows) originating from the interosseous tendons (red arrows) and extending to the extensor tendon (green arrow).

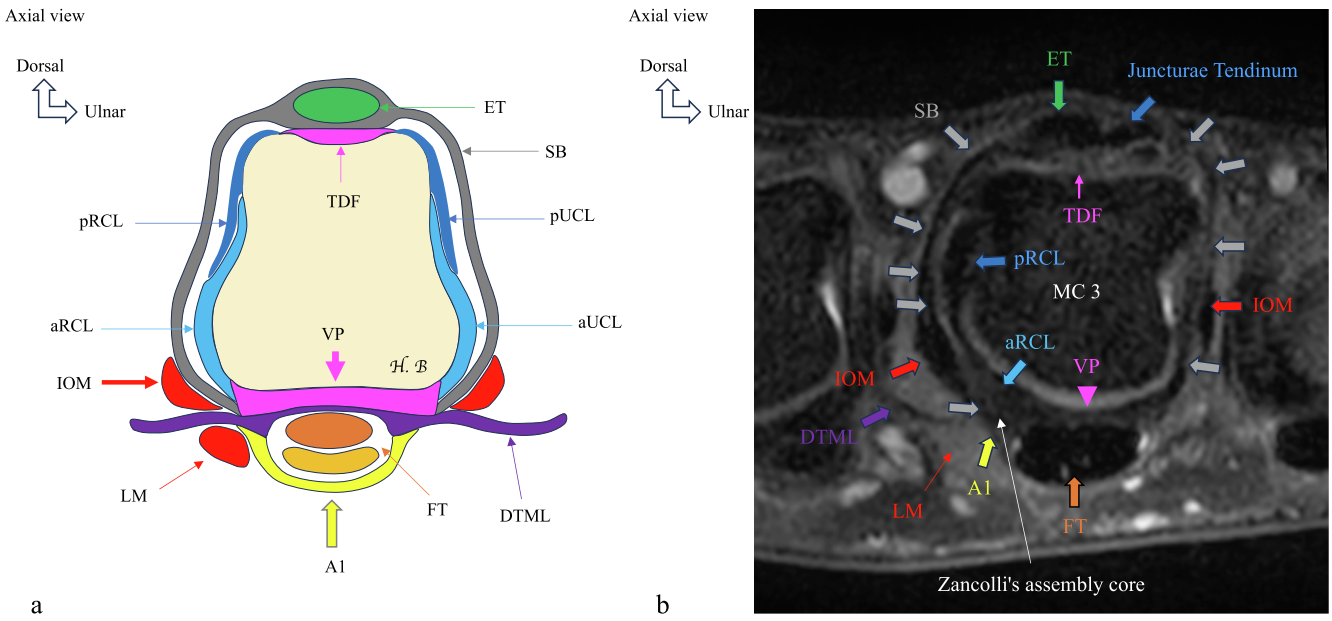

Fig. 26. Ligamentous, muscular, and tendinous structures of the middle finger MCPJ. Schematic drawing showing an axial cross-section (a). Axial proton density fat-suppressed (PD FS) MRI image (b). MC, metacarpal; P1, proximal phalanx; ET, extensor tendon; DTF, Dorsal triangular fibrocartilage; pRCL, principal radial collatéral ligament; pUCL, principal ullnar collatéral ligament; aRCL, accessory radial collateral ligament; aUCL, accessory ulnar collateral ligament; SB, sagittal bands; FT, flexor tendons; VP, volar plate; A1, A1 pulley; DTLM, deep transverse metacarpal ligament; IOM, interosseous muscles; LM, lumbrical Muscles.

facilitates rapid, objective, and reproducible assessment of synovial inflammation, particularly in rheumatoid arthritis [69].

5. Conclusion

This review article emphasizes the anatomical and imaging features of the MCPJ of the long fingers. Imaging provides excellent visualization of the various structures of the MCPJ of the long fingers and allows for dynamic assessment that correlates with biomechanics. Recognition of these structures on imaging and understanding their biomechanics form the foundation for appropriate clinical decision-making and therapeutic strategies. Looking forward, the MCPJ of the long fingers is well assessed by current imaging techniques, and further technological advancements in imaging modalities will enable even more detailed evaluation. We hope this review will serve as a guide for radiologists and surgeons and support future advanced research studies.

CRediT authorship contribution statement

Hicham Bouredoucen: Writing – original draft, Resources, Methodology, Investigation, Formal analysis, Data curation, Conceptualization. **Sana Boudabbous:** Supervision, Project administration. **Pierre-Alexandre Poletti:** Supervision, Project administration. **Lokmane Taihi:** Writing – review & editing, Supervision, Methodology, Conceptualization.

Declaration of competing interest

The authors declare that they have no known competing financial interests or personal relationships that could have appeared to influence the work reported in this paper.

References

[1] Condamine JL. Arthroplasties digitales métacarpophalangiennes et interphalangiennes proximales. EMC, Techniques chirurgicales-Orthopédie-Traumatologie, 44-374, 2002, 16 p.
[2] Rouvière H, Delmas A. Anatomie humaine : descriptive, topographique et fonctionnelle. Membres [Human Anatomy: descriptive, topographical, and functional. Limbs]. Elsevier Masson ;2002. 30-40. French.
[3] C.J. Dy, S.M. Tucker, P.L. Kok, K.A. Hearns, M.G. Carlson, Anatomy of the radial collateral ligament of the index metacarpophalangeal joint, J Hand Surg Am. 38 (1) (2013 Jan) 124–128.
[4] Y.C. Sun, X.M. Sheng, J. Chen, Z.W. Qian, In vivo metacarpophalanageal joint collateral ligament length changes during flexion, J Hand Surg Eur 42 (6) (2017 Jul) 610–615.
[5] L.M. Rozmaryn, The Collateral Ligament of the Digits of the Hand: Anatomy, Physiology, Biomechanics, Injury, and Treatment, J Hand Surg Am. 42 (11) (2017 Nov) 904–915.
[6] T. Kataoka, H. Moritomo, J. Miyake, T. Murase, H. Yoshikawa, K. Sugamoto, Changes in shape and length of the collateral and accessory collateral ligaments of the metacarpophalangeal joint during flexion, J Bone Joint Surg Am. 93 (14) (2011 Jul 20) 1318–1325.
[7] E. Zancolli, Structural and dynamic bases of hand surgery, 2nd edn., Lippincott Company, Philadelphia, 1979.
[8] J.K. Dickson, D.M. Evans, Reconstruction of the radial collateral ligament of the metacarpophalangeal joints of the fingers, Eur J Plast Surg 36 (2013) 307–314.
[9] P.S. Walker, M.J. Erkman, Laboratory evaluation of a metal-plastic type of metacarpophalangeal joint prosthesis, Clin Orthop Relat Res. 112 (1975 Oct) 349–356.
[10] H. Bade, J. Koebke, A. Nieden, Radiologic anatomy of the metacarpophalangeal joints II to V, Surg Radiol Anat. 19 (5) (1997) 323–327.
[11] Landsmeer jm. the coordination of finger-joint motions., J Bone Joint Surg Am. 45 (1963 Dec) 1654–1662.
[12] B. Jobbins, A.A. Amis, A. Unsworth, Biomechanics of the upper limb, in: D. Dowson, V. Wright (Eds.), An Introduction to the Biomechanics of Joints and Joint Replacement, Mechanical Engineering Publications, Ltd., London, 1981, pp. 97–102.
[13] A. Minami, K.N. An, W.P. Cooney 3rd, R.L. Linscheid, E.Y. Chao, Ligamentous structures of the metacarpophalangeal joint: a quantitative anatomic study, J Orthop Res. 1 (4) (1984) 361–368.
[14] K. Lutsky, J. Matzon, L. Walinchus, D.A. Ross, P. Beredjiklian, Collateral ligament laxity of the finger metacarpophalangeal joints: an in vivo study, J Hand Surg Am. 39 (6) (2014 Jun) 1088–1093.
[15] al-Qattan MM, Robertson GA. An anatomical study of the deep transverse metacarpal ligament. J Anat. 1993 Jun;182 (Pt 3)(Pt 3):443-6.
[16] J.F. Dubousset, Finger rotation during prehension, in: R. Tubiana (Ed.), The Hand, Vol. 1, Saunders, Philadelphia, PA, 1981, p. 202.
[17] Gratzer J, Vökt CA, Brenner P. Morphologische und funktionelle Zusammenhänge zwischen palmarer Platte der Metakarpophalangealgelenke und Binnenmuskulatur der Hand [Morphological and functional interface between palmar plates of metacarpophalangeal joints and intrinsic muscles of the hand]. Handchir Mikrochir Plast Chir. 2001 Sep;33(5):299-309. German.
[18] D.J. Hunter-Smith, P.G. Slattery, A. Rizzitelli, et al., The Dorsal Triangular Fibrocartilage of the Metacarpophalangeal Joint: A Cadaveric Study, J Hand Surg Am. 40 (7) (2015 Jul) 1410–1415.

[19] G.M. Rayan, D. Murray, K.W. Chung, M. Rohrer, The extensor retinacular system at the metacarpophalangeal joint. Anatomical and histological study, J Hand Surg Br. 22 (5) (1997 Oct) 585–590.
[20] M. Ishizuki, Traumatic and spontaneous dislocation of extensor tendon of the long finger, J Hand Surg Am. 15 (6) (1990 Nov) 967–972.
[21] C.M. Young, G.M. Rayan, The sagittal band: anatomic and biomechanical study, J Hand Surg Am. 25 (6) (2000 Nov) 1107–1113.
[22] B. Sivakumar, D.J. Graham, M. Hile, R. Lawson, Sagittal Band Injuries: A Review and Modification of the Classification System, J Hand Surg Am. 47 (1) (2022 Jan) 69–77.
[23] Hawthorne BC, Wellington IJ, Davey AP ett al. Suture Tape Augmentation for the Repair of Index Finger Radial Collateral Ligament Injury: A Biomechanical Study. J Hand Surg Am. 2024 Feb;49(2):179.e1-179.e7.
[24] K. Arai, S. Toh, K. Nakahara, S. Nishikawa, S. Harata, Treatment of soft tissue injuries to the dorsum of the metacarpophalangeal joint (Boxer's knuckle), J Hand Surg Br. 27 (1) (2002 Feb) 90–95.
[25] D.B. Kettelkamp, A.E. Flatt, R. Moulds, Traumatic dislocation of the long-finger extensor tendon. A clinical, anatomical, and biomechanical study, J Bone Joint Surg Am. 53 (2) (1971 Mar) 229–240.
[26] H.K. Watson, J. Weinzweig, P.M. Guidera, Sagittal band reconstruction, J Hand Surg Am. 22 (3) (1997 May) 452–456.
[27] Bonnel F. Anatomie des muscles interosseux et lombricaux de la main [Anatomy of the interosseous and lumbrical muscles of the hand]. Ann Chir Main. 1983;2(2): 172-8. French.
[28] K. Wang, E.P. McGlinn, K.C. Chung, A biomechanical and evolutionary perspective on the function of the lumbrical muscle, J Hand Surg Am. 39 (1) (2014 Jan) 149–155.
[29] J.S. Crowley, M. Meunier, R.L. Lieber, R.A. Abrams, The Lumbricals Are Not the Workhorse of Digital Extension and Do Not Relax Their Own Antagonist, J Hand Surg Am. 46 (3) (2021 Mar) 232–235.
[30] B.R. Campbell, M. Wu, J.M. Kistler, B.A. Hozack, M. Rivlin, C.M. Jones, Anatomic Relationship of Hand Intrinsic Tendons at the Metacarpal Head as It Relates to the Diagnosis of Saddle Syndrome: A Cadaveric Study, J Hand Surg Am. 50 (2) (2025 Feb) 232.e1–232.e6.
[31] N. Boutry, A. Lardé, X. Demondion, B. Cortet, H. Cotten, A. Cotten, Metacarpophalangeal joints at US in asymptomatic volunteers and cadaveric specimens, Radiology. 232 (3) (2004 Sep) 716–724.
[32] R.G. Gaston, G.M. Lourie, Radial collateral ligament injury of the index metacarpophalangeal joint: an underreported but important injury, J Hand Surg Am. 31 (8) (2006 Oct) 1355–1361.
[33] Lourie GM, Hanson ZC. Finger Metacarpophalangeal Joint Injuries in Athletes: Evaluation, Diagnosis, Treatment, and Return to Play. J Am Acad Orthop Surg. 2023 Feb 15;31(4):e177-e188.
[34] Revol M, Servant JM. Paralysie des muscles intrinsèques des doigts longs [Paralysis of the intrinsic muscles of the hand]. Chir Main. 2008 Feb;27(1):1-11. French.
[35] R. Tubiana, J.M. Thomine, E. Mackin, *Skeleton of the hand*, in: M. Dunitz (Ed.), *Examination of the Hand and Wrist*, Mosby, St Louis, Mo, 1996, pp. 3–28.
[36] M.B. Aguilá, J.S. Carné, A.H. Lluch, Rupture of the ulnar collateral ligament of the metacarpophalangeal joint of the index finger, J Hand Surg Br. 25 (1) (2000 Feb) 108–109.
[37] M. Ishizuki, Injury to collateral ligament of the metacarpophalangeal joint of a finger, J Hand Surg Am. 13 (3) (1988 May) 444–448.
[38] J.A. Masson, C.N. Golimbu, J.A. Grossman, MR imaging of the metacarpophalangeal joints, Magn Reson Imaging Clin N Am. 3 (2) (1995 May) 313–325.
[39] C.W. Pfirrmann, N.H. Theumann, M.J. Botte, J.L. Drapé, D.J. Trudell, D. Resnick, MR imaging of the metacarpophalangeal joints of the fingers: part II. Detection of simulated injuries in cadavers, Radiology. 222 (2) (2002 Feb) 447–452.
[40] N.H. Theumann, C.W. Pfirrmann, J.L. Drapé, D.J. Trudell, D. Resnick, MR imaging of the metacarpophalangeal joints of the fingers: part I. Conventional MR imaging and MR arthrographic findings in cadavers, Radiology. 222 (2) (2002 Feb) 437–445.
[41] G. Sakellariou, P.G. Conaghan, W. Zhang, et al., EULAR recommendations for the use of imaging in the clinical management of peripheral joint osteoarthritis, Ann Rheum Dis. 76 (9) (2017 Sep) 1484–1494.
[42] A.N. Colebatch, C.J. Edwards, M. Østergaard, et al., EULAR recommendations for the use of imaging of the joints in the clinical management of rheumatoid arthritis, Ann Rheum Dis. 72 (6) (2013 Jun) 804–814.
[43] Szkudlarek M, Østergaard M, Klarlund M, et al. Ultrasonography of the metacarpophalangeal and proximal interphalangeal joints in rheumatoid arthritis: a comparison with magnetic resonance imaging, conventional radiography and clinical examination. Arthritis Res Ther. 2003;5(5):R170–R176. doi:10.1186/ar1904.
[44] A.D. Brumbaugh, C. Quirk, J. Long, Painless swelling of the 3rd metacarpophalangeal joint, Skeletal Radiol. 53 (8) (2024 Aug) 1661–1662.
[45] Brewerton da., Hand deformities in rheumatoid disease, Ann Rheum Dis. 16 (2) (1957 Jun) 183–197.
[46] M. Kichouh, M. De Maeseneer, T. Jager, et al., Ultrasound findings in injuries of dorsal extensor hood: correlation with MR and follow-up findings, Eur J Radiol. 77 (2) (2011 Feb) 249–253.
[47] B.P. Kleinhenz, B.D. Adams, Closed Sagittal Band Injury of the Metacarpophalangeal Joint, J Am Acad Orthop Surg. 23 (7) (2015 Jul) 415–423.
[48] M. Fenech, Boxer's knuckle: Sonographic anatomy and assessment of sagittal band tears of the dorsal hood, Australas J Ultrasound Med. 26 (4) (2023 Oct 12) 216–229.
[49] S.M. Shepherd, E.Y. Chang, J.L. Rutledge, B. Huang, D. Trudell, D.L. Resnick, Cartilage assessment of the metacarpophalangeal joints: cadaveric study with magnetic resonance arthrography and finger traction, Clin Imaging. (2013 Jul-Aug; 37(4):718–22.).
[50] A. Gilbert, Palmar fibrocartilage lesions, in: P. Brüser, A. Gilbert (Eds.), Finger bone and joint injuries, Martin Dunitz, London, 1999, pp. 241–244.
[51] T. Hirano, M. Nishide, N. Nonaka, et al., Development and validation of a deep-learning model for scoring of radiographic finger joint destruction in rheumatoid arthritis, Rheumatol Adv Pract. (2019). Nov 22;3(2):rkz047.
[52] T. Hügle, E. Rosoux, G. Fahrni, D. Markham, T. Manigold, F. Becce, Development of a deep learning model for automated detection of calcium pyrophosphate deposition in hand radiographs, Front Med (Lausanne). 23 (11) (2024 Oct) 1431333.
[53] L. Caratsch, C. Lechtenboehmer, M. Caorsi, et al., Detection and Grading of Radiographic Hand Osteoarthritis Using an Automated Machine Learning Platform, ACR Open Rheumatol. 6 (6) (2024 Jun) 388–395.
[54] L. Folle, T. Meinderink, D. Simon, et al., Deep learning methods allow fully automated segmentation of metacarpal bones to quantify volumetric bone mineral density, Sci Rep. 11 (1) (2021 May 6) 9697.
[55] K.S. Stok, et al., Consensus approach for 3D joint space width of metacarpophalangeal joints using high-resolution peripheral quantitative computed tomography, Quant Imaging Med Surg. 11 (3) (2020) 691–701.
[56] R. Klose-Jensen, K.K. Keller, B. Langdahl, E.M. Hauge, Acceptance and image quality of high-resolution peripheral quantitative computed tomography of the metacarpophalangeal joints in rheumatoid arthritis, Int J Rheum Dis. 24 (12) (2021 Dec) 1473–1481.
[57] S.T. Ulas, K. Ziegeler, S.T. Richter, et al., Contrast-enhanced CT techniques and MRI perform equally well in arthritis imaging of the hand: a prospective diagnostic accuracy study, Eur Radiol. 32 (9) (2022 Sep) 6376–6383.
[58] S. Ogiwara, T. Fukuda, R. Kawakami, H. Ojiri, K. Fukuda, Anatomical analysis of inflammation in hand psoriatic arthritis by Dual-Energy CT Iodine Map, Eur J Radiol Open. 14 (8) (2021 Oct) 100383.
[59] A. Babulal Vadher, A. Sinha, S. Roy Choudhury, et al., Ultrasound and magnetic resonance imaging of hands in systemic sclerosis: A cross-sectional analytical study of prevalence of inflammatory changes in patients with subclinical arthropathy, J Scleroderma Relat Disord. 8 (1) (2023) 72–78.
[60] M.C. Fiorentino, E. Cipolletta, E. Filippucci, W. Grassi, E. Frontoni, S. Moccia, A deep-learning framework for metacarpal-head cartilage-thickness estimation in ultrasound rheumatological images, Comput Biol Med. 141 (2022) 105117.
[61] M. Wu, H. Wu, L. Wu, et al., A deep learning classification of metacarpophalangeal joints synovial proliferation in rheumatoid arthritis by ultrasound images, J Clin Ultrasound. 50 (2) (2022) 296–301.
[62] Y. Cheng, Z. Jin, X. Zhou, et al., Diagnosis of metacarpophalangeal synovitis with musculoskeletal ultrasound images, Ultrasound Med Biol. 48 (3) (2022) 488–496.
[63] A. Hashem, K.B. Al, The feasibility of high-resolution ultrasonography and MRI in diagnosing finger lesions, J Ultrasound. 25 (2) (2022) 133–144.
[64] C.N. Petchprapa, D. Vaswani, MRI of the Fingers: An Update, AJR Am J Roentgenol. 213 (3) (2019) 534–548.
[65] J. Ichikawa, H. Imada, K. Onohara, et al., Synovial chondromatosis: Rare involvement of metacarpophalangeal joint and diagnostic challenges in MR imaging, Skeletal Radiol. 53 (7) (2024) 1411–1415.
[66] Aydıngöz Ü, Yıldız AE, Ergen FB. Zero Echo Time Musculoskeletal MRI: Technique, Optimization, Applications, and Pitfalls. Radiographics. 2022 Sep-Oct;42(5):1398-1414.
[67] E. Laistler, B. Dymerska, J. Sieg, et al., In vivo MRI of the human finger at 7 T, Magn Reson Med. 79 (1) (2018) 588–592.
[68] T. Bayer, M.J. Brockhoff, A.M. Nagel, et al., Evaluation of finger cartilage composition in recreational climbers with 7 Tesla T2 mapping magnetic resonance imaging, Front Sports Act Living. 5 (2023) 1248581.
[69] Y. Mao, K. Imahori, W. Fang, et al., Artificial Intelligence Quantification of Enhanced Synovium Throughout the Entire Hand in Rheumatoid Arthritis on Dynamic Contrast-Enhanced MRI, J Magn Reson Imaging. 61 (2) (2025) 771–783.